Palaeogeography, Palaeoclimatology, Palaeoecology 661 (2025) 112697

Contents lists available at ScienceDirect

Palaeogeography, Palaeoclimatology, Palaeoecology

journal homepage: www.elsevier.com/locate/palaeo

Diverse ecological responses of foraminifera to the Middle Eocene Climatic Optimum (MECO) in shallow-water settings (Provençal Domain, NW Italy)

A. Gandolfi [a,*], V.M. Giraldo-Gómez [a,b], L. Arena [a], V. Luciani [c], C.A. Papazzoni [d], J. Pignatti [e], M. Piazza [a], L. Kocsis [f], C. Baumgartner [g], A. Briguglio [a]

[a] Dipartimento di Scienze della Terra, dell'Ambiente e della Vita, Università di Genova, Corso Europa 26, 16132 Genova, Italy
[b] Ellington Geological Services, 1414 Lumpkin Rd, 77043 Houston, USA
[c] Dipartimento di Fisica e Scienze della Terra, Università di Ferrara, Via Giuseppe Saragat 1, 44100, Ferrara, Italy
[d] Dipartimento di Scienze Chimiche e Geologiche, Università di Modena e Reggio Emilia, Via Campi 103, I-41125 Modena, Italy
[e] Dipartimento di Scienze della Terra, Università degli Studi di Roma "La Sapienza", Piazzale Aldo Moro 5, I-00185 Roma, Italy
[f] Institute of Earth Surface Dynamics, IDYST, University of Lausanne, Unil-Mouline, Geopolis, 1015 Lausanne, Switzerland
[g] Institute of Earth Sciences, ISTE, University of Lausanne, Unil-Mouline, Geopolis, 1015 Lausanne, Switzerland

ARTICLE INFO

Editor: L Angiolini

Keywords:
Marine calcifiers
Riverine influx
Bartonian
MECO
Palaeoecology

ABSTRACT

The Bartonian sedimentary succession of the drowning ramp of the Provençal-Dauphinois Domain records the Middle Eocene Climatic Optimum (MECO), the prominent global warming event, centered at ~40 Ma and lasting ~400–600 kyr. In this work, we study the response of foraminifera (planktic, smaller benthic and larger benthic foraminifera) as one of the main groups of marine calcifiers, highlighting their ecological behavior across the MECO climatic perturbation. Herein we present new data on the Olivetta San Michele section (NW Italy) across the MECO perturbance. We compare our findings with previous data from a wider geographic realm encompassing a large portion of the Provençal-Dauphinois ramp. The palaeoenvironmental reconstruction consists of slightly different depositional conditions in terms of riverine input, water depth, and distance from the mainland, which are reflected in faunal distribution. Nonetheless, the main part of the successions is interpreted as deposited within the photic zone and with a relatively high hydrodynamic regime. Planktic foraminiferal assemblages differ in the investigated successions both in abundance and diversity, suggesting major differences in the studied shallow-water setting. The variations in abundance of *Subbotina* and *Acarinina* appear to be controlled by both the MECO warming and a moderate increase of eutrophic conditions, related to an enhanced hydrological cycle. Shallow benthic communities, being already adapted to seasonal variations in salinity and temperature, proved to be resilient to long-term climatic perturbation. Their population shifts appear indeed directly impacted by changes in sedimentary rates and nutrient input modulated by the new hydrological cycle, in turn largely triggered by the warming.

1. Introduction

The early Paleogene is one of the most climatically dynamic periods of Earth's history, characterized by long-term warming and by several superimposed short-term warming events (~50–200 kyr), known as hyperthermals (Zachos et al., 2001). In the Eocene, the peaks of temperature and pCO_2 were reached during the Early Eocene Climatic Optimum (EECO, ~53–49 Ma) (Zachos et al., 2008; Huber and Caballero, 2011; Hollis et al., 2012; Inglis et al., 2015, 2020; Anagnostou et al., 2016; Hönisch et al., 2023). A long-term cooling trend (~49 to ~34 Ma) followed the EECO, eventually leading to the establishment of a continental Antarctic ice sheet by the early Oligocene (Coxall et al., 2005). This climatic transition was interrupted by a significant, though transient, global warming event: the Middle Eocene Climatic Optimum (MECO, ~40 Ma). During the MECO, the $\delta^{18}O$ values of marine carbonates and benthic foraminiferal shells declined by roughly 1 ‰ over ~400 kyr; this has been usually interpreted as a 4–6 °C global temperature rise, with a gradual onset and a brief temperature peak at ~40 Ma, followed by a rapid return to pre-event conditions (Bohaty and Zachos, 2003; Jovane et al., 2007; Bohaty et al., 2009; Edgar et al., 2010; Luciani et al., 2010; Spofforth et al., 2010; Savian et al., 2013; Boscolo Galazzo et al., 2014; D'Onofrio et al., 2021). Several characteristics, such as its

* Corresponding author.
E-mail address: antonella.gandolfi@edu.unige.it (A. Gandolfi).

https://doi.org/10.1016/j.palaeo.2024.112697
Received 23 July 2024; Received in revised form 3 December 2024; Accepted 27 December 2024
Available online 29 December 2024

duration being longer than the early Eocene hyperthermals, the absence of a clear trigger mechanism, and the lack of a globally coherent negative $\delta^{13}C$ excursion in marine carbonates, make the MECO one of the most enigmatic events in the Cenozoic, dubbed the middle Eocene "carbon cycle conundrum" (Sluijs et al., 2013). It has been suggested that the MECO warming was triggered by an atmospheric CO_2 increase by paroxysmal continental arc volcanism (e.g., van der Boon et al., 2021), even though the timing is not well constrained.

Considering that the MECO shares several characteristics with possible future climate changes (Representative Concentration Pathway RCP 8.5; Intergovernmental Panel on Climate Change, 2023), the evaluation of marine ecosystems resilience across this event is extremely significant. A population is resilient when it is able to resist a disturbance (e.g., via migration) and/or recover from disturbance (Capdevila et al., 2020) by returning to a stable state (Hodgson et al., 2015). The ongoing anthropogenic CO_2 emissions induce ocean acidification, eutrophication, and increased anoxia, thus compromising the marine ecosystem's resilience (Raven et al., 2005; Cooley et al., 2023). However, the present observations necessarily lack the long-term perspective offered by the geological record.

The interplay between global and regional climate processes and the resilience of the biosphere across the MECO have been mainly documented for deep-water settings (Ivany et al., 2008; Luciani et al., 2010; Boscolo Galazzo et al., 2014; Rivero-Cuesta et al., 2019; Marchegiano and John, 2022). The deep-water settings so far analyzed, though not recording evolutionary originations or extinctions, document pronounced variations within the biotic communities. In contrast, shallow-water depositional settings, such as carbonate platforms, ramps, or mixed carbonate-siliciclastic systems as recorded in the Mediterranean region (NW Tethys), are yet much less studied with respect to the MECO global climatic and environmental perturbations (Brachert et al., 2023; Gandolfi et al., 2023, 2024; Briguglio et al., 2024; Arena et al., 2024; Giraldo-Gómez et al., 2024).

With the aim of improving the understanding of the MECO impact on the shallow-water marine biotic communities, this study presents new data on the shallow-water sedimentary succession of Olivetta San Michele (OSM) cropping out in NW Italy (Fig. 1), near the Italian-French border. This section records a time interval that includes the MECO event and yields a diverse micro- and macrofauna composed of corals, mollusks, echinoids, foraminifera (both benthic and planktic), coccolithophores, and a large variety of ichnofossils as well. The presence of suspension feeders such as oysters, cardiid bivalves, and several detritus feeders intaking organic particles such as turritellid gastropods, suggests the occurrence of significant riverine input in this area. This diversity permitted an integrated approach to examine the effects of climate changes related to the MECO on shallow-water taxa, which are typically also controlled by other factors such as variations in hydrological cycles and related continental weathering, seafloor irradiation, and trophic conditions (Martín-Martín et al., 2021; Coletti et al., 2021; Brandano and Tomassetti, 2022; Bosellini et al., 2022; Briguglio et al., 2024). In a much broader framework, the data obtained are correlated with those from other sedimentary successions in the region, specifically the Sealza section (SE) and the Capo Mortola section (CM), published by Gandolfi et al. (2023), Coletti et al. (2021) and Gandolfi et al. (2024), respectively. The palaeogeographic setting of the foredeep basin of the Ligurian Alps (Italy) within the Provençal Domain proved to be an excellent playground where the MECO resilience of marine organisms can be traced.

2. Geological setting

The OSM succession is located near the village of Olivetta San Michele (Imperia province) (43°52′46.9"N 7°31′58.5″E) (Fig. 1). The studied deposits are part of the Meso-Cenozoic cover of the Provençal

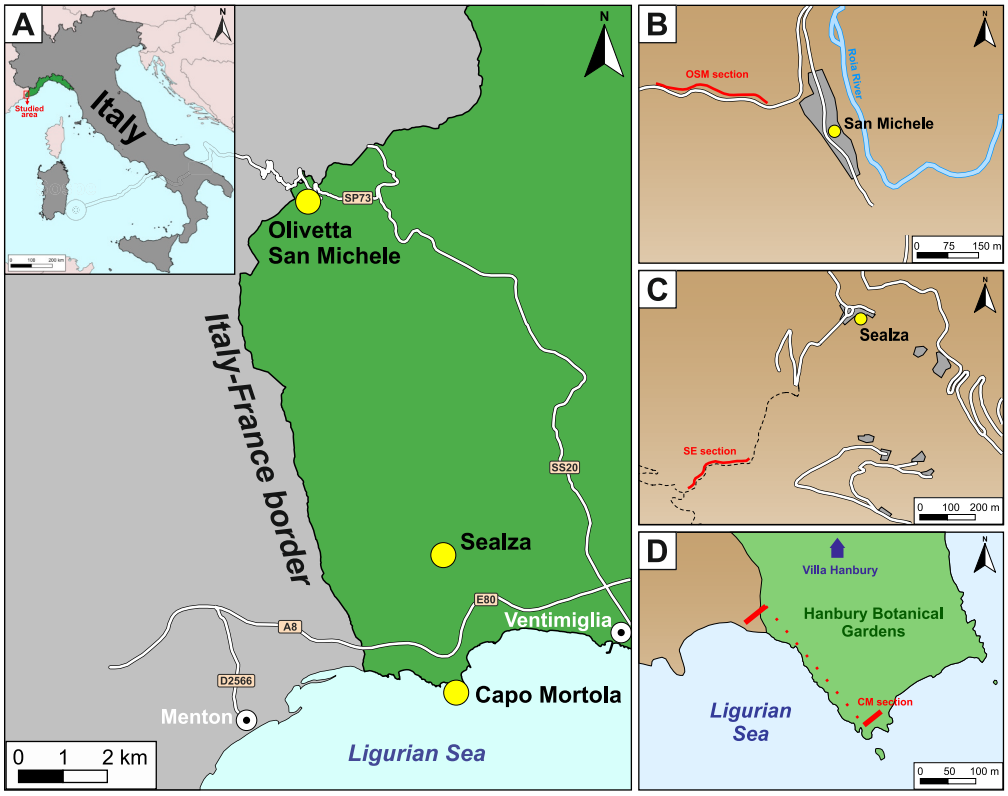

Fig. 1. a: Studied area (red rectangle) with geographic location of the three sections here discussed; **b:** Detail of the Olivetta San Michele (OSM) section; **c:** Detail of the Sealza (SE) section; **d:** Detail of the Capo Mortola (CM) section. (For interpretation of the references to colour in this figure legend, the reader is referred to the web version of this article.)

Domain that represents the southernmost part of the European Plate (Giammarino et al., 2010; Dallagiovanna et al., 2012; Seno et al., 2012; Decarlis et al., 2014; Marini et al., 2022). The sedimentation in this area was tectonically affected, being involved in the Pyrenean-Provençal (Cretaceous-Paleogene) and Alpine (Paleogene-Neogene) orogenic events, in the anticlockwise rotation and translation of the Corsica-Sardinia block (upper Oligocene-Miocene) and subsequently, in Pliocene to Recent tectonic events (de Graciansky et al., 2010; Dallagiovanna et al., 2012; Morelli et al., 2022). During the Paleogene tectonic phase, sediments are represented by shallow-water limestones grading upward to marlstones capped by siliciclastic turbidite deposits; this succession is known as the "trilogie priabonienne" (Boussac, 1912) or the "Sinclair trilogy" (Sinclair, 1997). The lithostratigraphic succession of this sector of the Provençal Domain includes in stratigraphic order: marls and marly limestones (Trucco formation: Campanian-lower Maastrichtian), *Microcodium*-rich, burrowed marls with grayish to reddish patches and minor conglomerates (*Microcodium* formation: upper Lutetian-lower Bartonian), biocalcirudites, biocalcarenites and minor fine- to coarse-grained siliciclastic deposits of shallow marine environment (Capo Mortola Calcarenite formation: lower Bartonian); marls, silty marls and very fine sandstones (Olivetta San Michele Silty Marl formation: Bartonian-lower Priabonian); siliciclastic turbidite deposits (Ventimiglia Flysch formation: upper Bartonian-lower Priabonian) (Giammarino et al., 2010; Dallagiovanna et al., 2012; Perotti et al., 2012; Brandano, 2019; Briguglio et al., 2024).

The MECO event along this sedimentary sequence was first hypothesized by Brandano and Tomassetti (2022) and only recently fully constrained both biostratigraphically and isotopically by Gandolfi et al. (2023, 2024), and Arena et al. (2024).

3. Material and methods

The OSM section has been previously described in terms of macro- and microfacies by Arena et al. (2024) and Giraldo-Gómez et al. (2024). In this study, we present new data on the uppermost interval of the succession from 190.0 m to 223.3 m (Fig. 2) as it records the MECO climatic perturbation. From this interval, we collected 20 rock samples, subsequently processed for foraminiferal and calcareous nannofossil analysis. In addition, 99 powder samples were collected from the outcrop surface using a pressure driller for stable carbon and oxygen isotope analysis.

Larger benthic foraminifera (LBF) were studied from rock thin sections obtained from fresh surface cuts. Only nummulitids could be properly identified according to the monograph of Schaub (1981) and, for axial sections, the work of Kleiber (1991).

Planktic (PF) and smaller benthic foraminifera (SBF) were extracted

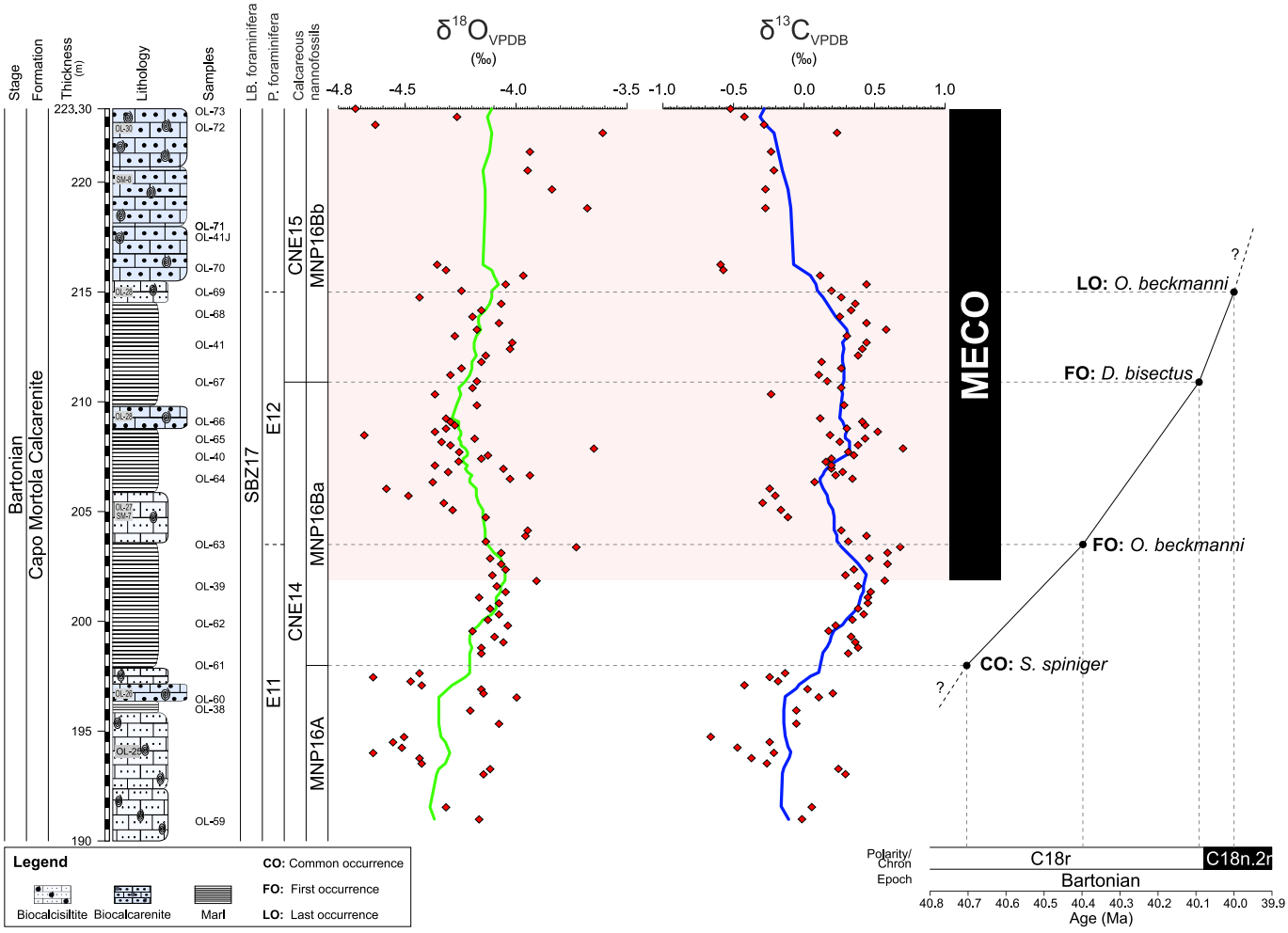

Fig. 2. $\delta^{18}O$ and $\delta^{13}C$ isotope data from bulk-sediment plotted against the stratigraphic log of the OSM section and biozones of LBF (SBZ: Serra-Kiel et al., 1998), PF (E: Wade et al., 2011), and calcareous nannofossil (MNP: Fornaciari et al., 2010 and CNE: Agnini et al., 2014). Green and blue lines indicate 5 point moving average. Biostratigraphy and age model of the OSM section for the middle Eocene based on calcareous nannofossil and planktic foraminifera events. Composite standard reference section (CSRS) of the middle Eocene (Bartonian) showing the absolute age model of Speijer et al. (2020). The pink-shaded band outlines the MECO interval, which also crosses the C18r and the C18n 2n, according to Speijer et al. (2020). (For interpretation of the references to colour in this figure legend, the reader is referred to the web version of this article.)

from rock samples using the acetic acid or acetolysis technique (Lirer, 2000; D'Onofrio and Luciani, 2020) that has been successfully applied to lithified rocks (Fornaciari et al., 2007; Luciani et al., 2007; Coccioni et al., 2012; Luciani and Giusberti, 2014; D'Onofrio et al., 2016; Luciani et al., 2016). Microfossils were picked, isolated in microslides, and identified under a binocular stereomicroscope (Optech GZ808) equipped with an on-board DeltaPix camera by Invenio, model 6EIII. The taxonomic criteria adopted in this study to identify SBF genera are based on Loeblich and Tappan (1987, 1994) and Holbourn et al. (2013), whereas PF taxa were identified according to Pearson et al. (2006).

The abundance of foraminiferal taxa was standardized to 1 g of dried sediment and expressed as a percentage to highlight changes in foraminiferal communities. The standardized abundance data were used to perform a Principal Components Analysis (PCA) using the PAST software (Hammer et al., 2001), merging the data here presented with those available in the literature from the region. LBF are not included in the statistical counting.

Coccolithophorids were retrieved from fourteen samples of the OSM section and observed in smear-slides following Bown and Young (1998). Semi-quantitative data were obtained by the observation under transmitted-light microscopy (Leitz) in cross-polarized (XPL) and phase contrast (PC) light at ~1000 magnification. The scarcity of calcareous nannofossil content reflects the shallow-water depositional environment. Semi-quantitative data were recorded by scanning five traverses of each slide, and five abundance classes were recorded (Gandolfi et al., 2023): very abundant, VA: taxon with abundances >50 % of the assemblage; abundant, A: 5 specimens per field of view (FOV); common, C: 1–4 specimens per FOV; few, F: 1 specimen per 1–10 FOVs; and rare, R: 1 specimen per >10 FOVs. Calcareous nannofossils were identified at species level whenever possible, following the taxonomy of Perch-Nielsen (1985) and Nannotax (Young et al., 2022). This study adopted the biozonations MNP (Fornaciari et al., 2010) and CNE (Agnini et al., 2014).

The 99 powdered samples were analyzed for $\delta^{13}C$ and $\delta^{18}O$ in the stable isotope laboratory of the University of Lausanne (Switzerland). The analyses were done on a Gasbench II coupled to a Finnigan MAT Delta V mass spectrometer by reacting the samples with phosphoric acid at 70 °C (Spötl and Vennemann, 2003). The generated CO_2 was introduced with a He-flow into the mass spectrometer. In-house Carrara Marble standards calibrated to NBS-19 were used to normalize the obtained data. The analytical precision for this method was better than the ±0.1 ‰ standard deviation. Cathodoluminescence (CL) images were obtained in a Technosyn 8200 MkII, which was operated at 15–20 kV and 0.4–0.5 mA with an unfocused cold cathode electron beam under a He atmosphere at 0.2 Torr. The Technosyn was mounted on an Olympus BH-2 microscope equipped with a DP 74 Olympus camera.

We analyzed the $\delta^{13}C$ and $\delta^{18}O$ records of shells of selected PF taxa (*Acarinina* spp., *Subbotina* spp., *Morozovelloides* spp., *Turborotalia* spp., *Globigerinatheka* spp., and *Orbulinoides beckmanni* (Saito, 1962)) to derive insight on their palaeobiology. Analyses were performed from the CM section (sample CM-45 in Gandolfi et al. (2024)) and from the tropical Atlantic Ocean Drilling Program (ODP) Site 1051 (samples 68.26 m below sea floor and 66.76 mbsf). We selected Site 1051 for its latitude comparable with that of the Liguria sections, allowing us to compare our shallow-water findings with those from deeper environments and to identify similarities or differences. The stable isotope analyses were conducted at the Stable Isotope Laboratory of the Department of Geosciences at Padova University using a Thermo Scientific Delta V Advantage Isotope Ratio Mass Spectrometer coupled with a Gas Bench II automated preparation device. Around 20–30 specimens per taxon were picked from the washed residue to make an isotope analysis.

4. Results

4.1. Foraminifera

The foraminiferal abundance within the disaggregated samples from the OSM section is scarce, and the preservation of SBF and PF tests is very poor. However, it has been possible to detect diagnostic morphological features useful to identify the genera and sometimes the species. Two of the samples (OL41J and OL72) processed for foraminiferal picking were barren. The abundances of SBF and PF are shown in Fig. 3, and the most significant taxa are shown in Fig. 4.

4.1.1. Smaller benthic foraminifera

A total of six SBF genera were recognized (Fig. 3). The most abundant is the genus *Heterolepa* (*H. dutemplei;* mean abundance 39.76 %), which remains constant in the interval from 196 to 214 m but starts to decrease in abundance from 214 to 217.5 m and subsequently shows an increase in the last sample at 223.2 m. The genus *Anomalinoides* (mean abundance 2.02 %) is absent in the lower and upper parts of the section, but it is present in the interval from 203.5 to 217.5, with an increase in abundance from 203.5 to 214 m followed by a decrease from 214 to 217.5 m. The genus *Cibicidoides* is scarcely represented in this section; it occurs only in three samples (OL66, OL67, and OL68) at 209.1 m, 210.9 m, and 214 m. The genus *Uvigerina* (mean value: 2.46 %) increases in abundance in the lower part of the section with a peak at 201.5 m, followed by a decrease in abundance from 201.5 to 211 m and a peak at 208.3 m. Other infaunal genera such as *Dentalina* and *Nodosaria* do not show significant changes in abundance but are present almost continuously from the base to the top of the interval analyzed. These genera have the same peak at 208.3 m as *Uvigerina*, even if *Dentalina* seems to be almost in antiphase compared to *Uvigerina*.

4.1.2. Larger benthic foraminifera

LBFs are infrequent in the herein investigated portion of the succession but they are more abundant and diverse in the lower part of the section. The assemblages are initially dominated by *Nummulites* ex gr. *perforatus* associated with sporadic *Assilina exponens* and rare *Discocyclina*; toward the middle part of the succession LBFs almost disappear, and they occur only as resedimented specimens. The uppermost 50 m of the succession yield mostly small operculinids, occurring sporadically, and very rare orthophragmines are present in the last meters. Throughout the succession, the LBF association is referable to SBZ 17 (Serra-Kiel et al., 1998).

4.1.3. Planktic foraminifera

As for PF, five taxa were identified: *Subbotina*, *Acarinina, Morozovelloides*, *Globigerinatheka*, and *Orbulinoides beckmanni*. The most abundant genus is *Subbotina* (mean abundance 34.18 %), which is recorded in all samples except for the barren ones (Fig. 3). This genus occurs rather constantly along the entire section. *Acarinina* is less abundant than *Subbotina* but shows an increase in abundance within the MECO (Fig. 3). *Globigerinatheka* is a minor component of the assemblages (mean abundance 1.21 %), it is present from 196 to 217.5 m with a minor shift and does not show significant variations. Finally, *Morozovelloides* appears only during the MECO interval with maximum abundance of only 2 %, and *O. beckmanni* is recorded by rare specimens in the interval spanning 203.5 to 215 m (samples OL63, OL65, OL66, and OL69).

Due to the occurrence of *O. beckmanni*, the Total Range Zone E12 (Wade et al., 2011) that largely corresponds to the MECO interval (Sexton et al., 2006; Bohaty et al., 2009), has been identified. The interval below the base of *O. beckmanni* is probably referable to Zone E11 due to the absence of *Guembelitrioides nuttallii*.

4.2. Calcareous nannofossils

The calcareous nannofossils in the OSM section are generally poorly

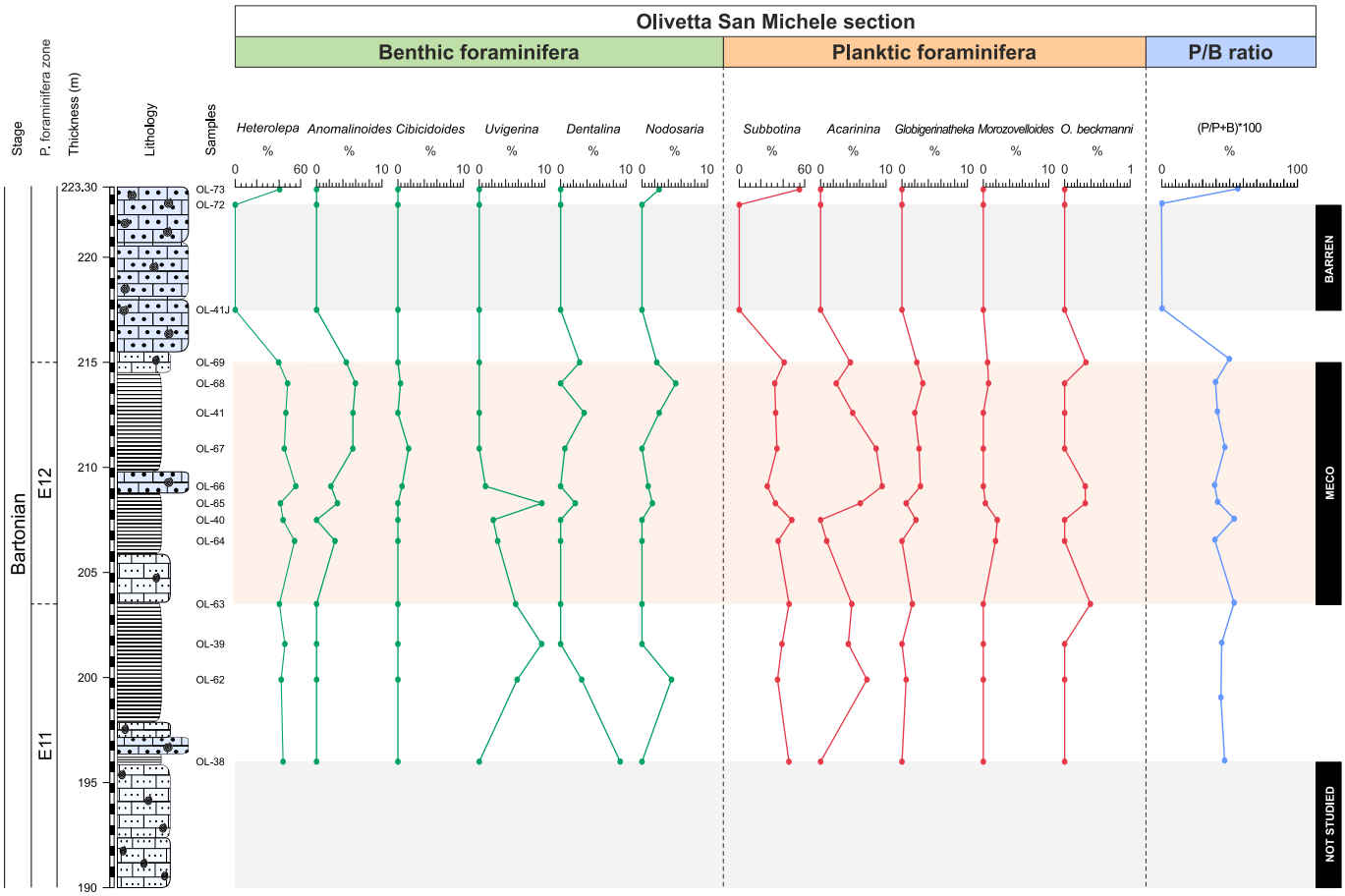

Fig. 3. Abundance of SBF and PF genera (>63 μm fraction) below, across, and above the MECO interval (pink-shaded band) in the OSM section, plotted against lithology and planktic foraminiferal biozones (Wade et al., 2011). (For interpretation of the references to colour in this figure legend, the reader is referred to the web version of this article.)

preserved and rather scarce, except for some marly layers (OL-62, OL-63) where they are more abundant and better preserved. In all samples, only a few reworked specimens of Cretaceous taxa are recorded. The most significant taxa are shown in Fig. 5. Two biozones have been identified (Fig. 2), according to the biozonation by Agnini et al. (2014). Biozone CNE14 is characterized by the common occurrence of *Reticulofenestra reticulata*, *R. umbilicus*, and *Sphenolithus furcatolithoides*. Biozone CNE15 is determined by the first occurrence of *Dictyococcites bisectus* in sample OL-67 (210.9 m), and this zone continues until the top of the studied section.

Likewise, two different biozones are recognized according to the biozonation by Fornaciari et al. (2010) (Fig. 2). Biozone MNP16A is identified due to the common presence of *S. furcatolithoides* and the occurrence of *R. reticulata* and *R. umbilicus*. Biozone MNP16B also includes the subzone MNP16Ba, defined by the continuous occurrence of *Sphenolithus spiniger* between the high occurrence (HO) of *S. furcatolithoides* and the lowest common occurrence (LCO) of *D. bisectus*. The common presence of *Dictyococcites scrippsae*, *R. reticulata*, *Coccolithus pelagicus*, and *Cyclicargolithus floridanus* is also recorded in this biozone. Finally, subzone MNP16Bb is determined by the FO of *D. bisectus* in sample OL-67 (210.9 m) and the common and continuous occurrence of *S. spiniger*. Other taxa recorded within this zone are *D. scrippsae*, *R. reticulata*, *C. pelagicus,* and *C. floridanus*. MNP16Bb correlates with biozone CNE15 and continues until the top of the studied section.

4.3. Carbon and oxygen stable isotopes in the OSM section

The results of bulk oxygen and carbon stable isotope analyses are shown in Fig. 2. The $\delta^{18}O_{bulk}$ values vary between −4.7 ‰ and − 3.9 ‰ but most of them are very close to −4.1 ‰, whilst the $\delta^{13}C_{bulk}$ values vary between 0.7 ‰ and − 0.7 ‰ with several minor shifts along the section. Between 190 and 202 m, the oxygen and carbon curves show the same positive trend followed by a negative shift. The carbon isotope data indicate relatively lower values toward the top of the succession whereas, the oxygen data show slightly more positive values.

The $\delta^{13}C$ and $\delta^{18}O$ values measured on *Acarinina* spp. and *Subbotina* spp. shells from sample CM-45 of the CM section (Gandolfi et al., 2024) show similar values, i.e., 1.0 vs. 0.9 ‰ and − 3.7 vs −3.8 ‰, respectively, very different from those obtained from Site 1051. Isotopic data from *O. beckmanni* are $\delta^{13}C = -1.1$ ‰ and $\delta^{18}O = -3.2$ ‰; however, an air peak invalidated the oxygen value, and no more specimens were available to repeat the analysis.

5. Discussion

5.1. MECO isotope data and their interpretation

The OSM section displays a $\delta^{18}O_{bulk}$ negative trend from 201.70 to 209.0 m. This negative excursion is included within the E12, CNE14 and 15 biozones, potentially related to the MECO event (Fig. 2; Bohaty and Zachos, 2003; Sexton et al., 2006; Edgar et al., 2007; Bohaty et al., 2009; Edgar et al., 2010; Boscolo Galazzo et al., 2014; Borelli et al., 2014; Giorgioni et al., 2019). The OSM age model displayed in Fig. 2 allows us to fix only the initial part of the MECO event. Data from CL show that the bulk of the studied lithologies in the OSM section are formed by clastic silt- and sand-sized elements, showing a diverse CL response ranging

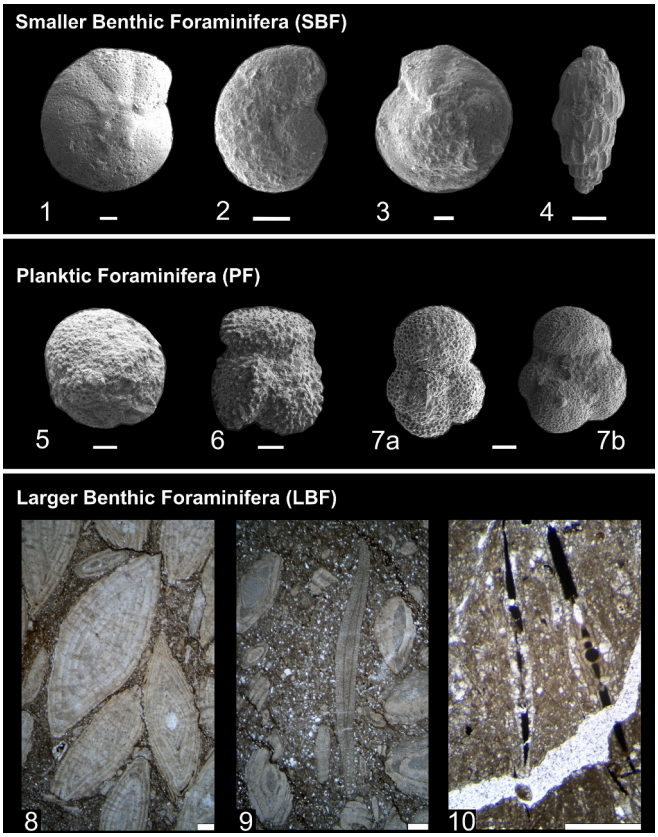

Fig. 4. Scanning electron microscope (SEM) images of the most significant taxa from the SE and CM sections (modified after Gandolfi et al., 2023, 2024) and thin sections of selected LBF from the OSM section. 1: *Heterolepa dutemplei* (d'Orbigny, 1846); 2: *Anomalinoides* sp.; 3: *Cibicidoides* sp.; 4: *Uvigerina* sp.; 5: *Orbulinoides beckmanni* (Saito, 1962); 6: *Acarinina praetopilensis* (Blow, 1979); 7a, b: *Subbotina hagni* (Gohrbandt, 1967). Scale bar = 100 μm.
8: *Nummulites* ex gr. *perforatus* (de Montfort, 1808); 9: *Discocyclina* sp.; 10: *Assilina exponens* (Sowerby, 1840). Scale bar = 500 μm.

from bright orange-yellow to dark violet (Fig. 6). This indicates a heterogeneous (possibly Cretaceous) origin of clasts, which were probably derived from the erosion of a pre-existing emerging rocky substrate further north in the domain. The SBF and PF exhibit an almost intrinsic dark blue to mauve, pristine CL (Fig. 6).

Samples from OSM record lower $\delta^{18}O$ values in comparison with the values from CM and SE sections (Gandolfi et al., 2023, 2024) (Fig. 7 A, B, C). However, the largely scattered values of measured $\delta^{13}C$ and $\delta^{18}O$ from the shallow-water sections of OSM, CM, and SE (Figs. 6A, 7) may suggest several intervals where pore water chemistry differs from the original seawater chemistry and the original isotopic signal has been altered (Veizer et al., 1999; Zachos et al., 2001; Giraldo-Gómez et al., 2017; Gandolfi et al., 2024) (Fig. 6).

A non-significant correlation (Pearson correlation coefficient $r \leq 0.3$) between $\delta^{13}C$ and $\delta^{18}O$ may indicate that a diagenetic overprint of the primary isotopic signal of carbonate can be excluded (Fio et al., 2010; Peris Cabré et al., 2023). The presence of pristine autochthonous bioclasts (foraminifera and probably nannofossils in the matrix) is responsible for the recorded negative trend similarly observed at OSM and at SE, which is highly diluted by isotopic values derived from a variety of calcareous lithoclasts. At CM this detrital influence has totally obliterated the negative tendency, and the $\delta^{18}O$ curve seems to follow lithological changes. The 1 ‰ offset between SE and OSM is a very minor effect of slightly different tectonic settings (Fig. 7 A, B, C). The lower values of $\delta^{18}O$ recorded in the three sections (Fig. 6A) may indicate some influence of burial diagenesis, which modified the oxygen isotope signature (Banner and Hanson, 1990; Marshall, 1992; Lavastre et al., 2011; Pellenard et al., 2014; Al-Mojel et al., 2018); nevertheless, the heterogeneity of CL response in some analyzed samples in the OSM section (OL-61, OL-64, OL-69, and OL-74) excludes very extensive burial diagenesis because the CL of the different components (litho- and bioclasts) has not been homogenized (Fig. 6 B). Some samples in the SE section record very low $\delta^{18}O$ and $\delta^{13}C$ values, probably indicating a strong influence of meteoric diagenesis (Fig. 6 A).

From a general perspective, it has been reported from multiple regions that negative values recorded in the $\delta^{18}O$ signal during the MECO are more common in shallow-water settings, where sediments are more sensitive to the diagenetic signal (e.g., Peris Cabré et al., 2023; Sharma et al., 2024) than in deep-water sites (Bohaty et al., 2009; Edgar et al., 2010; Spofforth et al., 2010).

5.2. Palaeoceanographic setting and palaeo-water depth reconstruction

Within the western Liguria geological and structural framework, characterized by a foreland-foredeep system (Marini et al., 2022 and references therein), the sections SE, CM, and OSM reflect a progressive deepening trend. A deepening of the depositional settings is also recorded in each succession from the base upwards. We infer this scenario based on both the taxonomic diversity of LBFs and the increasing percentage of PF to SBF ratio (P/B ratio; Fig. 3) (e.g., van der Zwaan et al., 1999).

At SE, very low values of P/B ratio are recorded in the lower part of the section, interpreted as implying palaeodepth <50 m, whereas in the MECO interval, the increase of the P/B ratio values (mean value 10 %) suggests palaeodepth possibly up to ~80 m (Gandolfi et al., 2023). This is also confirmed by the LBF assemblage, which is mostly dominated by thick *Nummulites* ex gr. *perforatus* tests and, toward the top, by thin operculinas (Briguglio et al., 2024) and by the absence of discocyclinids.

The CM section has P/B mean values greater than SE, being around 23 % (Gandolfi et al., 2024), whereas these values strongly increase in the OSM section (mean values 45 %, this work), thus indicating greater depths. The LBF assemblage in the CM section changes from thick and diverse nummulitid shells to large and flat assilinas and lastly to thin discocyclinids, thus expressing the full range of bathymetric realm for symbiont-bearing foraminiera, though always within the photic zone. LBF scarcity or absence in a large interval of the OSM section, including the MECO, is likely due to higher depth, probably within the oligophotic zone (Arena et al., 2024). An accurate palaeogeographic reconstruction is hampered by tectonic dislocation (de Graciansky et al., 2010; Dallagiovanna et al., 2012; Morelli et al., 2022); nevertheless, we suppose that the SE section was probably closer to the fluvial discharge and related nutrient input, as being the shallowest succession with thick conglomerates at its base directly above the Upper Cretaceous marly limestone. On the contrary, the dominant marly sediments of the OSM succession denote a finer terrigenous contribution, possibly due to the greater distance from the fluvial discharge and deeper setting.

5.3. How did shallow-water calcifiers react to the MECO event?

The main changes recorded in SBFs, LBFs, and PFs from the shallow-water Liguria successions are summarized in Fig. 8. Both seafloor settings and upper water column environments are mainly interpreted from the known ecological characters of the taxa recorded. The palaeoenvironmental reconstruction of the Bartonian Liguria ramp allows us to evaluate the degree of adaptation of the various biotic communities to the MECO event and to test their degree of resilience, if any, to the climate warming.

5.3.1. Smaller benthic foraminifera

The most pronounced changes in SBF assemblages are recorded from the shallowest SE section (Fig. 8). The genus *Cibicidoides* is highly abundant in the pre-MECO interval, thus suggesting a well-oxygenated

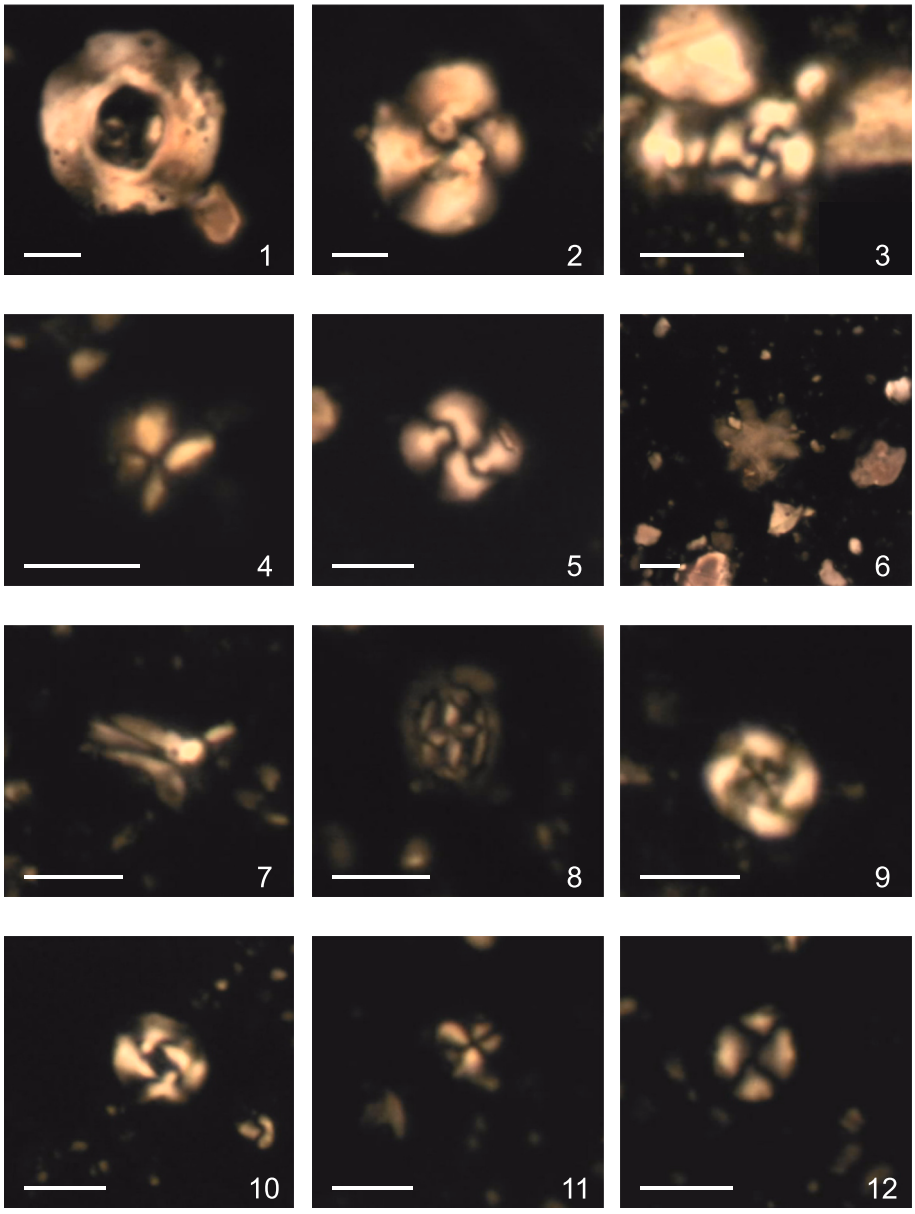

Fig. 5. Photomicrographs of selected calcareous nannofossils from the OSM section. Scale bar = 5 μm in all figures 1. *Reticulofenestra umbilicus*; 2. *Dictyococcites bisectus*; 3, 5. *Dictyococcites scrippsae*; 4, 11. *Sphenolithus spiniger*; 6. *Discoaster* sp.; 7 *Sphenolithus furcatolithoides*; 8. *Campylosphaera dela*; 9. *Reticulofenestra reticulata*; 10. *Cyclicargolithus floridanus*; 12. *Coccolithus pelagicus*.

seafloor and poor nutrient supply. This genus is indeed recognized as an epifaunal, epiphytic benthic foraminifer living in well-oxygenated environments (Speijer, 1994; Speijer and Schmitz, 1998; Murray, 2006; Giraldo-Gómez et al., 2018a, 2018b). During the MECO event, *Cibicidoides* firstly decreases in abundance (Gandolfi et al., 2023), probably due to the oxygen reduction and rise in the organic flux associated with the MECO warming (Spofforth et al., 2010), as confirmed by the increase of the TOC values (Gandolfi et al., 2023). However, after the initial and marked decrease, *Cibicidoides* slowly adapted to the MECO perturbance as suggested by its abundance recovery toward the top of the event (Gandolfi et al., 2023). This genus, outside its preferred ecological conditions, is able to adapt to reduced bottom-water oxygen concentrations (Rathburn et al., 2018; Schmiedl et al., 2023). Indeed, some species of *Cibicidoides* tolerate increased organic carbon fluxes and labile seasonal food supply (Licari, 2006).

The genus *Anomalinoides,* regarded as having ecological characters similar to *Cibicidoides* (van der Zwaan, 1982; Rögl and Spezzaferri, 2002; Russo et al., 2022), follows the same trend of *Cibicidoides* in the pre-MECO phase being very abundant, but it temporarily prevails over *Cibicidoides* across the MECO interval. Along the deeper CM section, these two genera are both present and do not display prominent changes during the MECO (Gandolfi et al., 2024).

In the deepest OSM section, both *Cibicidoides* and *Anomalinoides* are absent in the pre-MECO phase and increase constantly in abundance during MECO (Fig. 3). This abundance variation between *Cibicidoides* and *Anomalinoides* along a depth gradient might be related to ecological factors such as food availability, seawater chemistry, competition, and oxygen concentration (van der Zwaan et al., 1999), which were modified during the MECO event. The genus *Heterolepa*, known as preferring oxygenated waters as *Cibicidoides* and *Anomalinoides* (van der Zwaan, 1982; Rögl and Spezzaferri, 2002; Russo et al., 2022), occurs in all three sections. In the shallowest SE section, *Heterolepa* increases in abundance during the warming event, proving to be favored by the temperature increase (Fig. 8), while in the deeper CM and OSM sections, it is rather abundant throughout the investigated intervals (Fig. 3).

In the shallowest SE section, the decrease in oxygen content and

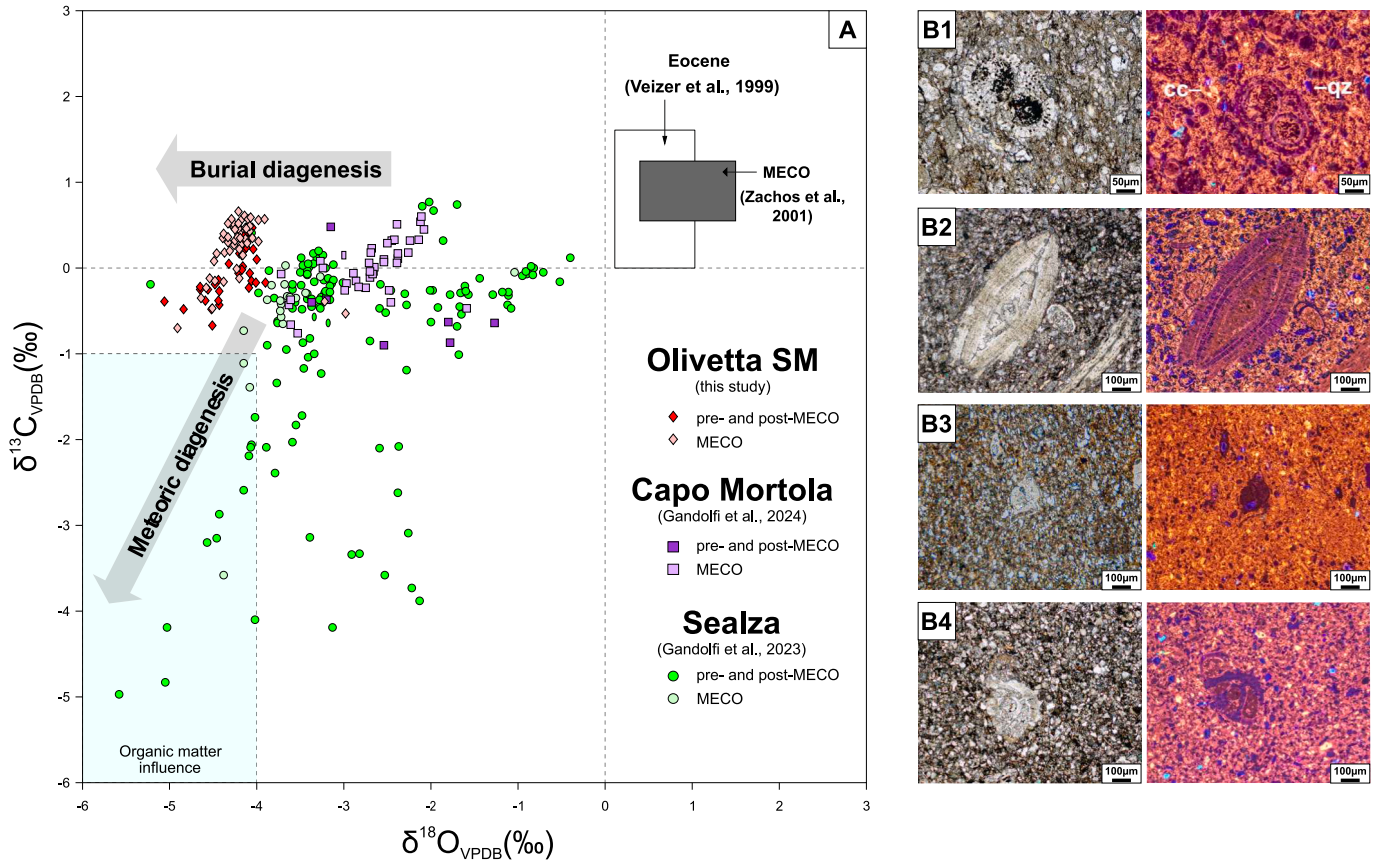

Fig. 6. A. Cross-plot of $\delta^{18}O$ against $\delta^{13}C$ of bulk-sediment from the three sections in the Provençal domain: OSM (this study), CM (modified after Gandolfi et al., 2024), and SE (modified after Gandolfi et al., 2023). Isotopic values showing the pathways that indicate the influence of burial and meteoric diagenesis (Lavastre et al., 2011; Pellenard et al., 2014; Al-Mojel et al., 2018). The $\delta^{13}C$ and $\delta^{18}O$ ranges are from Veizer et al. (1999) and Zachos et al. (2001) for the Eocene and MECO, respectively. **B.** Photomicrographs of representative of lithologies sampled in the OSM section (this study) showing the plane-polarized transmitted light (on the left, PPL) and cathodoluminescence (on the right, CL). **B1.** Sample OL74 is detrital packstone characterized by more abundant dull violet bioclasts including a planktic foraminifer, set in a bright orange matrix. **B2.** Sample OL71 is calcarenite quite rich in quartz grains (dark blue). The *Nummulites* test shows a well-preserved lamellar structure with mauve CL, attesting for little diagenetic overprint. **B3.** Sample OL69 is a calcisiltite dominated by bright orange carbonates in an orange matrix and a smaller benthic foraminifer with dark violet CL. **B4.** Sample OL61 is a calcisiltite dominated by silt-sized carbonate clasts with a mauve CL mixed with some bright foraminifera is again of dull violet CL indicating a mix of intrinsic and very low Mn^{2+} CL emission. (For interpretation of the references to colour in this figure legend, the reader is referred to the web version of this article.)

increase of organic matter preservation at the seafloor during the MECO may explain the increase in *Uvigerina* abundance because this genus is considered a proxy for carbon-rich and oxygen-poor conditions (Sen Gupta and Machain-Castillo, 1993; Kaiho, 1994; Thomas and Gooday, 1996; Schmiedl et al., 1997; van der Zwaan et al., 1986, 1999; De Rijk et al., 2000; Hess and Kuhnt, 2005; Kawagata et al., 2006). Conversely, in the deeper CM section, where abundant epifaunal benthic taxa prevailed, *Uvigerina* is relatively rare, possibly due to better oxygenated bottom waters and lower organic flux (Gandolfi et al., 2024). The OSM section records the same trend, as *Uvigerina* decreases in abundance until it disappears (Fig. 3). The scarcity of both porcelaneous and agglutinated foraminifera in our sections seems probably related to the great abundance of LBFs that may have prevented the establishment of a highly diversified community (Beavington-Penney and Racey, 2004; Kövecsi et al., 2022).

5.3.2. *Larger benthic foraminifera*

As expected from shallow-water successions, LBFs are generally the most abundant group of foraminifera present in all the studied stratigraphic sequences (Varrone, 2004; Coletti et al., 2021; Brandano and Tomassetti, 2022).

The genus *Nummulites* in the SE section is virtually the only LBF taxon during the pre-MECO, and it remains very abundant throughout the entire succession, followed by sporadically abundant small *Operculina* that appear only when the lithology gets finer and muddier, i.e. in marly limestones (Fig. 8) (Gandolfi et al., 2023; Briguglio et al., 2024). Since SE is considered the shallowest of all the investigated sections, it is reasonable to infer that only LBFs adapted to this shallow depth occur and dominate. Interestingly, in the entire SE succession, porcelaneous foraminifera, which are typical of the shallowest environments, are completely absent (Briguglio et al., 2024). Possibly *Nummulites* was more tolerant to a somewhat increased of nutrient levels than the porcelaneous foraminifera, confined to strictly oligotrophic waters (Beavington-Penney and Racey, 2004; Kövecsi et al., 2022). In the CM section, the LBF assemblage, dominated initially by *Nummulites* spp., shifts to an *Assilina exponens* assemblage just before the MECO interval, and finally *Discocyclina* spp. co-dominating with *Assilina exponens* and small operculinas during the entire MECO event (Gandolfi et al., 2024). These variations could be attributed to the deepening-upward conditions and changes in seafloor irradiation, as *Assilina* and especially *Discocyclina* are commonly considered to be able to inhabit the lower photic zone (e.g., Beavington-Penney and Racey, 2004).

In OSM the genus *Nummulites* is rather abundant in the lowest part of the succession (Arena et al., 2024; Giraldo-Gómez et al., 2024), followed by sparse *Assilina*, *Operculina*, and *Discocyclina*, appearing just before the MECO. All these taxa decrease in abundance and almost disappear across the MECO interval, where they are only recorded as resedimented

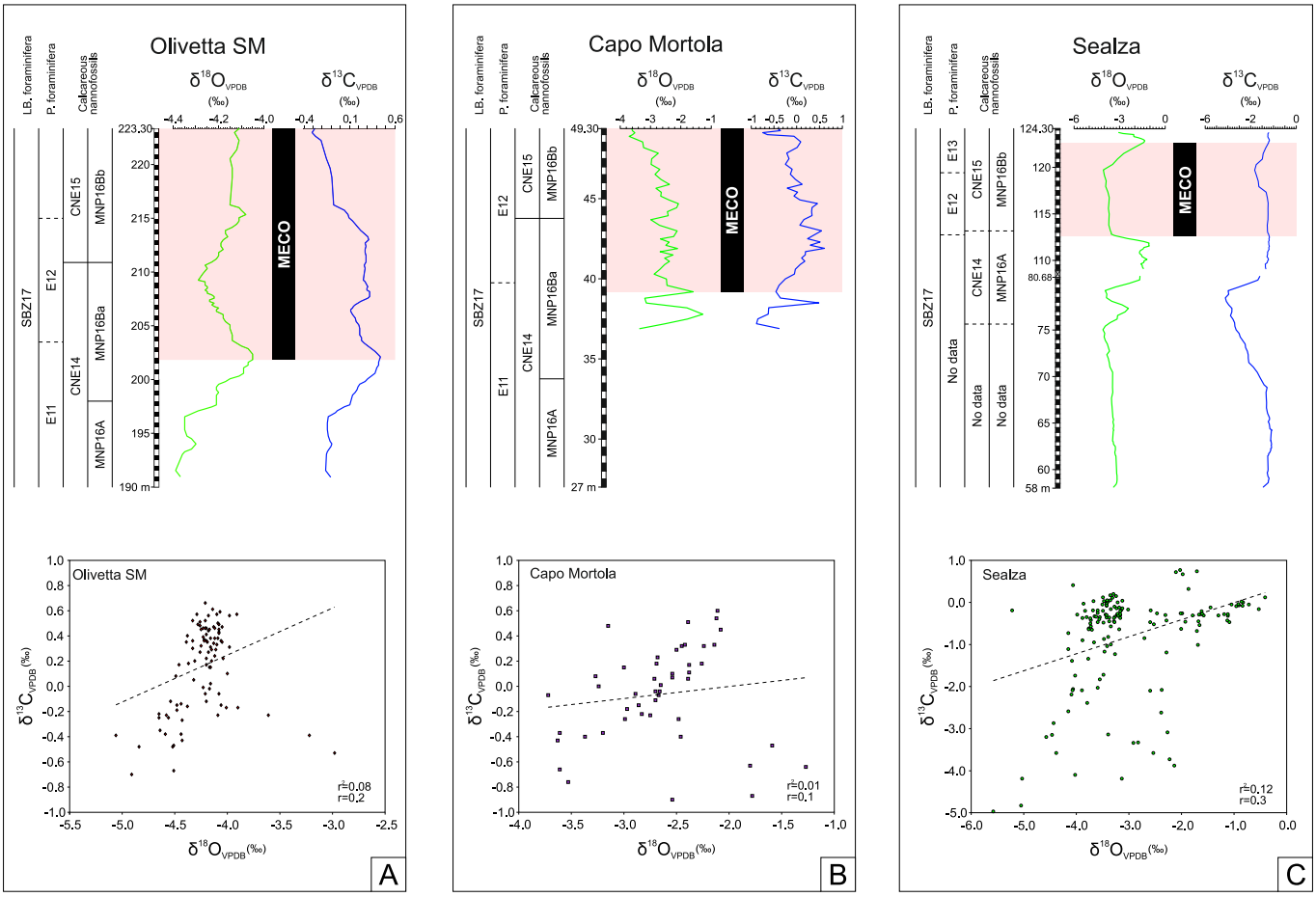

Fig. 7. Isotope data ($\delta^{18}O$: green line; $\delta^{13}C$: blue line) from the Ligurian sections in the Provençal domain (all using 5 point moving average compilations) with respective cross-plots (using original data) between $\delta^{18}O$ and $\delta^{13}C$ showing the Pearson correlation and regression. **A.** OSM section (this study). **B.** CM section (modified after Gandolfi et al., 2024). **C.** SE section (modified after Gandolfi et al., 2023). (For interpretation of the references to colour in this figure legend, the reader is referred to the web version of this article.)

material (Giraldo-Gómez et al., 2024). This sudden disappearance can be interpreted as a consequence of the deepening trend that brought this locality well below the photic zone where no LBF can thrive, and all tests are transported from shallower environments (Fig. 8).

In conclusion, our data highlight that the LBF assemblages respond more promptly to irradiation conditions at the seafloor rather than to MECO-related temperature variations. Irradiation at the seafloor may have been controlled, besides the water depth, by water turbidity likely due to enhanced fluvial input, in turn related to an accelerated hydrological cycle across the MECO.

5.3.3. *Planktic foraminifera*

In the analyzed shallow-water successions, mainly dominated by LBF, PF are generally scarce; nonetheless, they increase in abundance in the upper part of all the three sections (Fig. 8). In the shallowest SE section, PF in the pre-MECO phase are generally rare, with the cold-water index genus *Subbotina* (e.g., Boersma et al., 1987) being the most common taxon. During the MECO interval, the simultaneous decrease in abundance of *Subbotina* coupled with a significant increase in abundance of *Acarinina* and the sudden appearance of *Morozovelloides* likely suggest an increase of the surface-water temperature because these two taxa are indicating mixed-layer, oligotrophic warm-waters that dominated the tropical and subtropical assemblages in the late Paleocene to middle Eocene (with *Morozovella* preceding *Morozovelloides*) (Boersma et al., 1987; Pearson et al., 1993, 2001; Edgar et al., 2010). Even in the OSM section a slight increase in *Acarinina* is observed across the MECO, though its abundance remains lower than in SE and significantly lower as compared to *Subbotina* (Fig. 8). Conversely, at the CM section, *Acarinina* shows a marked decrease in abundance during the MECO phase, which may appear unusual for this genus, which prefers warm environments (e.g., Boersma et al., 1987; Pearson et al., 1993, 2001, 2006). *Acarinina* has indeed been recorded to increase in abundance during early Paleogene hyperthermals and the EECO (Agnini et al., 2009; Luciani et al., 2016; D'Onofrio et al., 2021; Filippi et al., 2024), but it decreased during the MECO in bathyal Tethyan successions (Luciani et al., 2010; D'Onofrio et al., 2021). This reduction across the MECO has been linked to increased surface-water eutrophy (Luciani et al., 2010; D'Onofrio et al., 2021; Gandolfi et al., 2024), that in the CM section possibly affected the habitat of the specialized, oligotrophic mixed-layer dweller acarininids (e.g., Boersma et al., 1987; Pearson et al., 1993, 2001, 2006).

The relatively common occurrence of the deep-water thermocline dweller *Subbotina* (e.g., Pearson et al., 2006) in the studied sections may appear atypical, especially in the shallower SE and CM sections. However, *Subbotina* has been recorded as capable of moving its habitat higher in the upper column, as suggested from Northwest Atlantic Site U1408 by the middle Eocene stable isotope data close to the surface water dwellers (Kearns et al., 2021). Our stable isotope data, from the CM section (CM-45 Gandolfi et al., 2024), confirm that *Subbotina* lived in a surface-water habitat across the MECO as the $\delta^{18}O$ and $\delta^{13}C$ values are close to those obtained for the mixed-layer *Acarinina* (Fig. 9). The genus *Subbotina* is not only recognized as a cold-water index, but it may also indicate meso- to eutrophic conditions (D'Onofrio et al., 2021 and references therein). In CM and OSM sections during the MECO, the genus

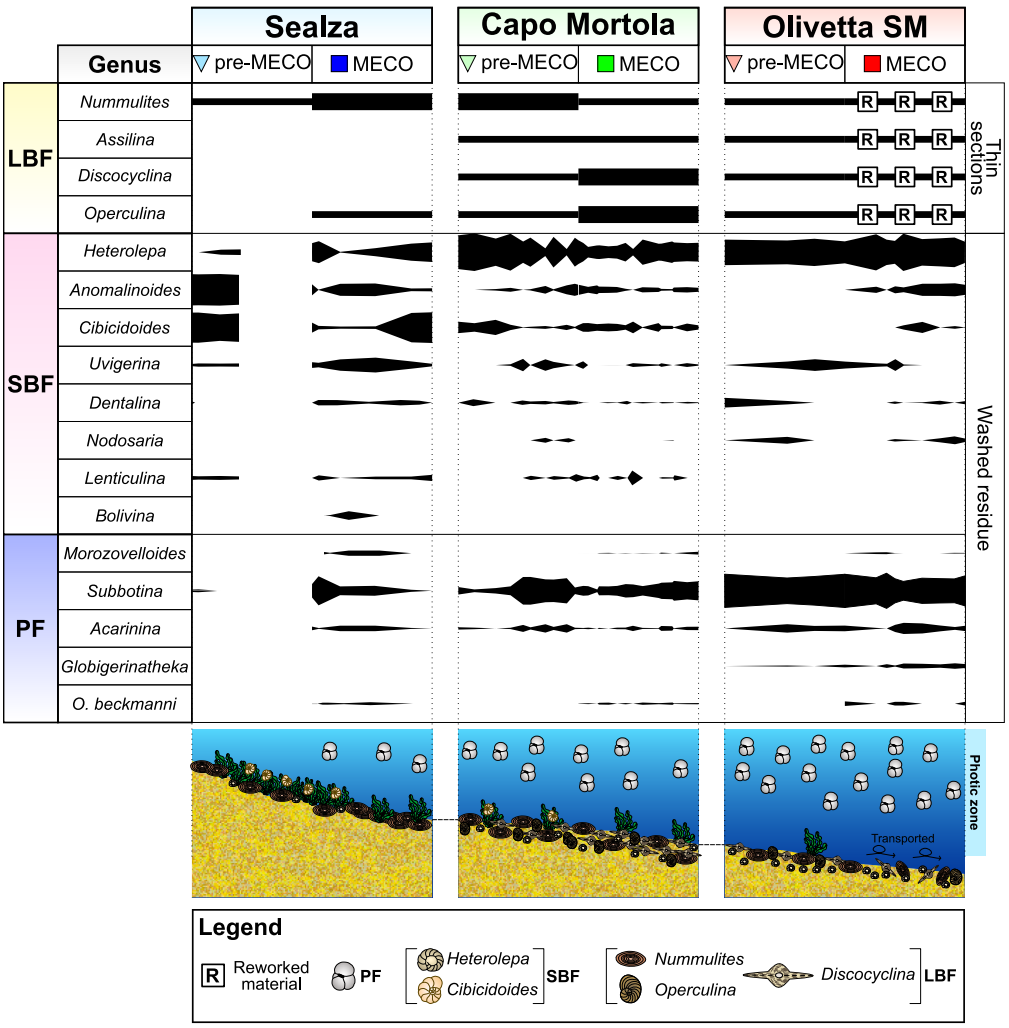

Fig. 8. Comparative scheme for biodiversity and palaeodepth estimation across all investigated sections. PF: planktic foraminifera, SBF: smaller benthic foraminifera, LBF: larger benthic foraminifera. See text for further details.

Subbotina displays an initial slight decrease interrupted by a positive trend toward the top of the section (Gandolfi et al., 2024). We suppose that *Subbotina* was initially affected by the MECO warming, but afterwards it benefited from the nutrient supply related to the enhanced hydrological cycle, commonly associated with this event (Luciani et al., 2010; D'Onofrio et al., 2021; Gandolfi et al., 2023, 2024).

A further peculiar response is recorded by the genus *Globigerinatheka*, which is completely absent in the SE and CM sections and occurs with scattered specimens only in the OSM section (Figs. 3, 8) (Gandolfi et al., 2023, 2024). This absence/scarcity is unusual because this genus is regarded as having a habitat comparable with that of *Acarinina* and possibly *O. beckmanni.* (Boersma et al., 1987; Pearson et al., 1993; Premoli Silva and Jenkins, 1993; Pearson et al., 2001, 2006; Wade and Kroon, 2002; Wade, 2004). However, the ecological characteristics of *O. beckmanni* are unclear, lacking stable isotope data. It is assumed to share the *Globigerinatheka* habitat due to morphological similarities and because it is believed descending from *Globigerinatheka euganea* (Pearson et al., 2006). Our new stable isotope data obtained at the CM section and Site 1051 (Fig. 9) may suggest an alternative explanation. Although the CM specimens are affected by greater test recrystallization than those from Site 1051, they record evident differences between the isotope values from the taxa analyzed. The lower $\delta^{13}C$ values from *O. beckmanni* than *Globigerinatheka* and *Acarinina,* recorded at the Atlantic Site 1051 and CM (~2 ‰), suggest it may have inhabited slightly deeper waters or had less efficient symbiosis relationships with respect to the other two genera (Fig. 9). With these differences, it is possible that the ecological characters of *O. beckmanni* advantaged it in the Liguria setting across the MECO. The possible shallow-water habitat of *Subbotina* may provide a further explanation for the scarcity/absence of *Globigerinatheka*, as the former may have prevailed in the ecological competition for vital resources, invading to some extent the *Globigerinatheka* ecological niche.

5.3.4. *Calcareous nannofossils*

The calcareous nannofossils were only semi-quantitatively estimated in all three sections. Preservation is generally poor in most of the analyzed samples with variable degrees of overgrowth and recrystallization, so assemblages documenting pristine conditions are rare to few.

Notwithstanding, we attempt to derive information on variations in the photic zone based on the recognized ecological affinities of the taxa recorded. Though differences arise from the three sections, the assemblages share some common characters (Gandolfi et al., 2023, 2024). Specifically, enhanced eutrophy at the MECO can be deduced by the rarity or virtual absence of oligotrophic taxa such as *Sphenolithus furcatulithoides*, *Cyclicargolithus floridanus*, and *Zygrhablithus bijugatu,* with the latter also known as a cold water index (e.g., Young, 1998; Aubry, 1998; Bralower, 2002; Agnini et al., 2007; Gibbs et al., 2004; D'Onofrio et al., 2021). The increase in abundance of the warm watereutrophic index *Dictyococcites scrippsae* is only recorded at the SE section, whereas the other eutrophic and warm indices such as *Coccolithus pelagicus* and

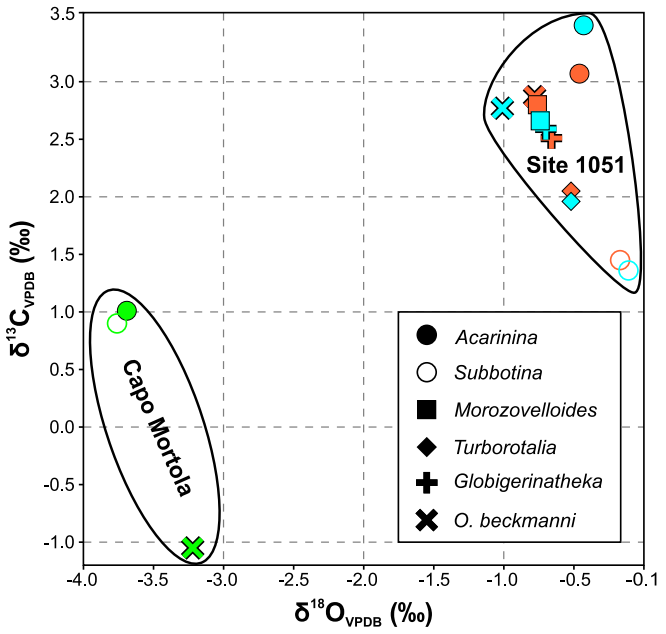

Fig. 9. Cross-plot of $\delta^{18}O$ against $\delta^{13}C$ values for selected taxa analyzed from sample CM-45 (green) across the MECO interval and from ODP Site 1051 (orange for 66.76 m depth and light blue for 68.26 m depth). (For interpretation of the references to colour in this figure legend, the reader is referred to the web version of this article.)

D. bisectus (Wei and Wise, 1989; Villa et al., 2008) do not display significant variations or occur only in the post-MECO interval. However, reworking of Cretaceous nannofossils increases across the MECO, especially in the two shallower SE and CM sections, indicating terrigenous discharge in the surface waters. Similar variations have been detected in the MECO of the Baskil section, Turkey (D'Onofrio et al., 2021) and may testify the increased fluvial input likely triggered by the MECO enhanced hydrological cycle that appears to have primarily affected the shallower successions rather than tectonics.

5.4. Palaeoecological and palaeoenvironmental reconstruction

We performed the PCA analysis for each section by using our standardized abundance data for SBF and PF, to check for possible ecological groupings that might further provide insights on the palaeoenvironmental reconstruction of the entire study area. The results are illustrated in Fig. 10 for all three sections.

In each analysis, there is a dense cloud of taxa all clustering very close to each other, which can be defined as the "MECO assemblage"; it is composed, in fact, by all those taxa that either appear suddenly or have a distinctive peak during the MECO event. The same group includes the species *O. beckmanni* and the genera *Acarinina* and *Morozovelloides*; the former taxon confirms that the MECO assemblage is indeed restricted to the MECO event, and both genera suggest that surface water temperature was a major trigger of such peculiar grouping. Further confirmation is given by the cold-water index *Subbotina* which always plots far from the MECO assemblage (Fig. 10). This confirms that PC1 indicates temperature, which rised at the MECO and was the main controlling factor of the assemblage. This peculiar pattern seems to be replicated almost identically in all three sections, thus confirming the general interpretation.

There are, however, some significant differences among the PCAs as suggested by the positioning of the genera *Cibicidoides* and *Heterolepa* which appear scattered in different parts of the diagram (Fig. 10). This pattern may reflect the diverse palaeogeographic position of each succession. As the SE section records the shallowest setting, the abundant LBF, corals and mollusks probably benefited from higher light

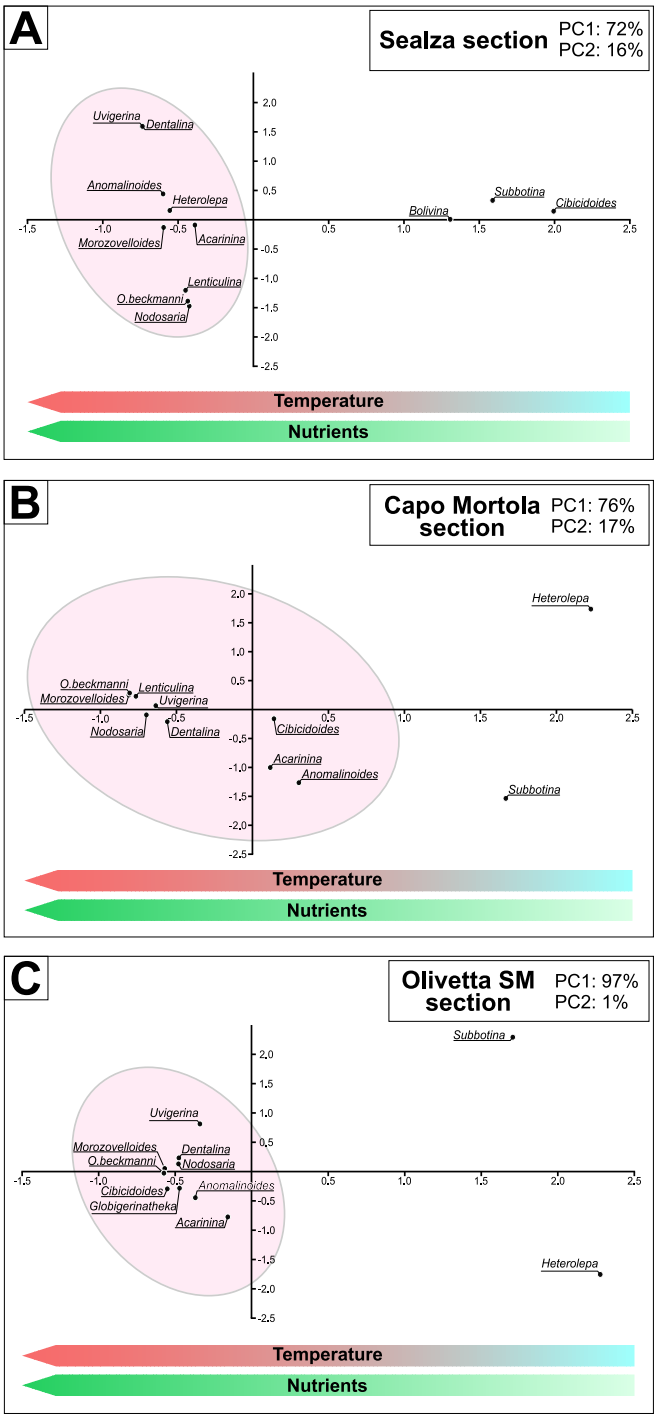

Fig. 10. Principal component analyses for the three studied sections. The pink ellipse represents the MECO assemblage. (For interpretation of the references to colour in this figure legend, the reader is referred to the web version of this article.)

penetration, and *Cibicidoides* may have thrived on highly vegetated seafloor in the pre-MECO interval. During the MECO, the dominance of *Heterolepa* and *Anomalinoides* at SE suggest greater ecological flexibility for these two genera with respect to *Cibicidoides*, abundant mostly in the pre-MECO phase and out of the MECO assemblage. (Fig. 10 a). In the CM section, *Heterolepa* falls far from *Cibicidoides,* thus indicating a contrasting response (Fig. 10 b). The anti-phase variations in abundance of these two genera may suggest possible ecological competitions never previously reported. In OSM, the PCA shows a marked distinction

between pre-MECO and MECO (Fig. 10 c), indicating the increasing difference between the two types of communities. This may suggest that rising temperatures and runoff, impacting nutrients and light availability, influenced benthic communities. The alternate occurrence of *Heterolepa* and *Cibicidoides* within the MECO grouping or outside of it (Fig. 10) indicates that these genera were resilient to the MECO environmental variations.

The most complex interpretation is related to the genus *Subbotina* as its position in the PCAs seems compatible with the cold preferences of this genus but appears in contrast with its affinities to eutrophic conditions (Fig. 10) as this taxon should not reflect a nutrient-poor environment (e.g., Boersma et al., 1987; D'Onofrio et al., 2021 and references therein). However, such a peculiar pattern can be explained with diverse degrees of adaptation and resilience; the eutrophic cold-water index *Subbotina* does not enter into the MECO assemblage due to the temperature increase, which probably exceeded its ecological tipping point, but the increasing mesotrophic settings could have favored its abundance. This interpretation implies that *Subbotina* was tolerant to the MECO climatic perturbation in these shallow-water settings as the undesired temperature increase was somewhat compensated by its preference for eutrophic conditions. Concerning LBF, they seem not to be particularly influenced by MECO temperature effects but appear to have been mostly affected by enhanced eutrophy and/or water turbidity, therefore occurring at the specific depths requested by their photosymbionts. In this context, a specific resilience of LBF to the climatic perturbation driven by MECO cannot be directly established; however, they remain important environmental indicators that can vary their abundance and diversity depending on the ecological conditions at the seafloor.

The supposed enhanced eutrophy to explain the calcareous plankton and LBF records in the three sections studied does not contrast with the general oligotrophic conditions recorded by SBF, dominated by epifaunal taxa, and whether nutrients were mainly consumed by the former groups. Elevated temperatures could have indeed enhanced the rate of bacterial respiration and remineralization significantly, thus resulting in more efficient recycling of nutrients higher in the water column (John et al., 2013, 2014; Ma et al., 2014). This would have resulted in a restriction of food supply at depth.

6. Summary and conclusions

This study illustrates the palaeoecological and palaeoenvironmental variations across the MECO event in shallow-water settings of western Liguria. In these settings, the interpretation of the recorded changes is complex due to constant perturbations from nearby riverine systems, superimposed on the warming trend, that affected the foraminiferal communities. These factors may hamper the observation of clear direct correlations between climate and biosphere because any higher sedimentary input might indeed have been derived by both tectonic activity and enhanced precipitations triggered by improved weathering, commonly associated with warming events. In addition, diagenetic effects were quite intense due to high sediment porosity, and therefore the interpretation of all isotopic data must be taken with caution. However, the correspondence of the biotic variations with the MECO $\delta^{18}O$ negative shifts suggests the significant contribution of the warming event on the fossil assemblages. Furthermore, the negative excursions are included within planktic foraminiferal biozone E12 as well as within the calcareous nannofossil biozones CNE14 and 15, which largely correspond to the time of the MECO event. Despite the above-listed difficulties, this work reveals diverse ecological flexibilities of the taxa recorded, mainly attributable to the climatic variations triggered by the MECO event.

Our interpretations take also into account that data integration from all studied sites allows a reliable palaeogeographic reconstruction along a depth gradient, thus differentiating the shallower site of SE from the deeper ones of CM and OSM. Based on the variations recorded in both benthic and planktic communities, it is reasonable to suppose that, along with increasing temperatures, runoff was also crucial in the interpretation of MECO's impact on organisms' ecology, especially in the analyzed shallow-water settings. Runoff enhancement can lead to reduced irradiation on the seafloor, an increased sedimentation rate, and higher nutrient availability, thus affecting to a different extent the trophic behavior of the entire communities, favoring the more ecologically flexible taxa.

The MECO perturbance (considering both temperature and runoff) induced indeed major changes and diverse degrees of adaptations in benthic and planktic foraminiferal communities. Assemblages were modified by the MECO event to a different extent, thus proving that populations were generally not resistant to the disturbance by moving to a different state. In this scenario, some taxa, such as *Cibicidoides*, *Heterolepa*, and *Subbotina,* proved to be more resilient to the new environmental conditions, whereas LBFs were more affected by the other factors such as the decrease in seafloor irradiation, caused by either higher water turbidity or increased water depth.

CRediT authorship contribution statement

A. Gandolfi: Writing – review & editing, Writing – original draft, Visualization, Methodology, Investigation, Formal analysis, Data curation, Conceptualization. **V.M. Giraldo-Gómez:** Writing – review & editing, Writing – original draft, Investigation, Conceptualization. **L. Arena:** Writing – original draft, Visualization. **V. Luciani:** Writing – review & editing, Conceptualization. **C.A. Papazzoni:** Writing – review & editing. **J. Pignatti:** Writing – review & editing, Validation. **M. Piazza:** Writing – review & editing. **L. Kocsis:** Writing – review & editing, Methodology, Formal analysis. **C. Baumgartner:** Writing – review & editing, Methodology, Formal analysis. **A. Briguglio:** Writing – review & editing, Validation, Supervision, Resources, Funding acquisition, Conceptualization.

Declaration of competing interest

The authors declare that they have no known competing financial interests or personal relationships that could have appeared to influence the work reported in this paper.

Acknowledgements

This study was supported by the University of Genova, which funded a Curiosity Driven Project awarded to AB on Ligurian Palaeoenvironments and by the Ministry of Education, University and Research (MIUR), Italy, which awarded to AB, MP, VL and CAP a PRIN 2017 research project labelled "Biota resilience to global change: biomineralization of planktic and benthic calcifiers in the past, present and future" (prot. 2017RX9XXY), and a PhD PON Green awarded to AG. VL was supported by FAR 2023 and MP thanks FRA 2022/2023 at the University of Genova for the support of this project. We would like to thank Claudia Agnini (University of Padova) and Giulia Filippi (University of Ferrara) for their lab work on isotope analysis. We also thank the editor and two anonymous reviewers for their constructive comments, which helped us to improve the manuscript.

Appendix A. Taxonomic appendix

A.1. Benthic foraminifera

Anomalinoides Brotzen, 1942.
Cibicidoides Thalmann, 1939.
Dentalina Risso, 1826.
Heterolepa Franzenau, 1884.
Heterolepa dutemplei (d'Orbigny, 1846).
Nodosaria Lamarck, 1816.

Uvigerina d'Orbigny, 1826.

A.2. Planktic foraminifera

Acarinina Subbotina, 1953.
Acarinina praetopilensis (Blow, 1979).
Globigerinatheka Brönnimann, 1952, emended Proto Decima & Bolli, 1970.
Morozovelloides Pearson & Berggren, 2006.
Orbulinoides beckmanni (Saito, 1962).
Subbotina Brotzen & Pożaryska, 1961.
Subbotina hagni (Gohrbandt, 1967) = *Parasubbotina hagni* (Gohrbandt 1967).

A.3. Larger benthic foraminifera

Assilina exponens (Sowerby, 1840).
Nummulites ex gr. *perforatus* (Montfort, 1808).

A.4. Calcareous nannofossils

Chiasmolithus Hay et al., 1966.
Chiasmolithus solitus (Bramlette & Sullivan, 1961) Locker, 1968.
Clausicoccus Prins, 1979.
Coccolithus pelagicus (Wallich, 1877) Schiller, 1930.
Cribrocentrum reticulatum (Gartner & Smith, 1967) Perch-Nielsen 1971 = *Reticulofenestra reticulata* (Gartner & Smith, 1967) Roth & Thierstein, 1972.
Cyclicargolithus floridanus (Roth & Hay, in Hay et al., 1967) Bukry, 1971.
Discoaster Tan Sin Hok, 1927.
Discoaster saipanensis Bramlette & Riedel, 1954.
Dictyococcites bisectus (Hay, Mohler & Wade, 1966) Bukry & Percival, 1971 = *Reticulofenestra bisecta* (Hay, Mohler & Wade, 1966) Roth, 1970.
Dictyococcites scrippsae Bukry & Percival, 1971.
Ericsonia Black, 1964.
Helicosphaera compacta Bramlette & Wilcoxon, 1967.
Pontosphaera Lohmann, 1902.
Reticulofenestra Hay, Mohler & Wade, 1966.
Reticulofenestra dictyoda (Deflandre in Deflandre & Fert, 1954) Stradner in Stradner & Edwards, 1968.
Reticulofenestra umbilicus (Levin, 1965) Martini & Ritzkowski, 1968.
Sphenolithus Deflandre in Grassé, 1952.
Sphenolithus furcatolithoides Locker, 1967.
Sphenolithus moriformis (Brönnimann & Stradner, 1960) Bramlette & Wilcoxon, 1967.
Sphenolithus predistentus Bramlette & Wilcoxon, 1967 = *Furcatolithus predistentus* (Bramlette & Wilcoxon, 1967) Howe 2021.
Sphenolithus spiniger Bukry, 1971.
Zygrhablithus bijugatus (Deflandre in Deflandre & Fert, 1954) Deflandre, 1959.

Appendix B. Supplementary data

Supplementary data to this article can be found online at https://doi.org/10.1016/j.palaeo.2024.112697.

Data availability

Data will be made available on request.

References

Agnini, C., Fornaciari, E., Rio, D., Tateo, F., Backman, J., Giusberti, L., 2007. Responses of calcareous nannofossil assemblages, mineralogy and geochemistry to the environmental perturbations across the Paleocene/Eocene boundary in the Venetian Pre-Alp. Mar. Micropaleontol. 63 (1–2), 19–38. https://doi.org/10.1016/j.marmicro.2006.10.002.

Agnini, C., Macrì, P., Backman, J., Brinkhuis, H., Fornaciari, E., Giusberti, L., Luciani, V., Rio, D., Sluijs, A., Speranza, F., 2009. An early Eocene carbon cycle perturbation at ~ 52.5 Ma in the Southern Alps: Chronology and biotic response. Paleoceanography 24 (2). https://doi.org/10.1029/2008PA001649.

Agnini, C., Fornaciari, E., Raffi, I., Catanzariti, R., Pälike, H., Backman, J., Rio, D., 2014. Biozonation and biochronology of Paleogene calcareous nannofossils from low and middle latitudes. Newsl. Stratigr. 47 (2), 131–181. https://doi.org/10.1127/0078-0421/2014/0042.

Al-Mojel, A., Dera, G., Razin, P., Le Nindre, Y.M., 2018. Carbon and oxygen isotope stratigraphy of Jurassic platform carbonates from Saudi Arabia: Implications for diagenesis, correlations and global paleoenvironmental changes. Palaeogeogr. Palaeoclimatol. Palaeoecol. 511, 388–402.

Anagnostou, E., John, E.H., Edgar, K.M., Foster, G.L., Ridgwell, A., Inglis, G.N., Pancost, R.D., Lunt, D.J., Pearson, P.N., 2016. Changing atmospheric CO2 concentration was the primary driver of early Cenozoic climate. Nature 533 (7603), 380–384 doi: 10.

Arena, L., Giraldo-Gómez, V.M., Baucon, A., Piazza, M., Papazzoni, C.A., Pignatti, J., Gandolfi, A., Briguglio, A., 2024. Short-term middle Eocene (Bartonian) paleoenvironmental changes in the sedimentary succession of Olivetta San Michele (NW Italy): the response of shallow-water biota to climate in NW Tethys. Facies 70 (4), 259–284. https://doi.org/10.1007/s10347-023-00677-4.

Aubry, M.P., 1998. Early Paleogene calcareous nannoplankton evolution: a tale of climatic amelioration. In: Aubry, M.P., Lucas, S.G., Berggren, W.A. (Eds.), Late Paleocene-Early Eocene Biotic and Climatic Events in the Marine and Terrestrial Records. Columbia University Press, New York, NY, USA, pp. 158–201.

Banner, J.L., Hanson, G.N., 1990. Calculation of simultaneous isotopic and trace element variations during water-rock interaction with applications to carbonate diagenesis. Geochim. Cosmochim. Acta 54 (11), 3123–3137.

Beavington-Penney, S.J., Racey, A., 2004. Ecology of extant nummulitids and other larger benthic foraminifera: applications in palaeoenvironmental analysis. Earth-Sci. Rev. 67 (3–4), 219–265.

Boersma, A., Premoli Silva, I., Shackleton, N.J., 1987. Atlantic Eocene planktonic foraminiferal paleohydrographic indicators and stable isotope paleoceanography. Paleoceanography 2, 287–331. https://doi.org/10.1029/PA002i003p00287.

Bohaty, S.M., Zachos, J.C., 2003. Significant Southern Ocean warming event in the late middle Eocene. Geology 31, 1017–1020. https://doi.org/10.1130/G19800.1.

Bohaty, S.M., Zachos, J.C., Florindo, F., Delaney, M.L., 2009. Coupled greenhouse warming and deep-sea acidification in the middle Eocene. Paleoceanography 24, PA2207. https://doi.org/10.1029/2008PA001676.

Borelli, C., Cramer, B.S., Katz, M.E., 2014. Bipolar Atlantic deep-water circulation in the middle- late Eocene: Effects of Southern Ocean gateway openings. Paleoceanography 29, 308–327. https://doi.org/10.1002/2012PA002444.

Boscolo Galazzo, F., Thomas, E., Pagani, M., Warren, C., Giusberti, L., 2014. The middle Eocene climatic optimum (MECO): a multi-proxy record of paleoceanographic changes in the southeast Atlantic (ODP Site 1263, Walvis Ridge). Paleoceanogr. Paleoclimatol. 29, 1143–1161.

Bosellini, F.R., Benedetti, A., Budd, A.F., Papazzoni, C.A., 2022. A coral hotspot from a hot past: the EECO and post-EECO rich reef coral fauna from Friuli (Eocene, NE Italy). Palaeogeogr. Palaeoclimatol. Palaeoecol. 607, 111284. https://doi.org/10.1016/j.palaeo.2022.111284.

Boussac, J., 1912. Études stratigraphiques sur le Nummulitique alpin. Serv. Carte Géol. Fr, Mém, p. 662.

Bown, P.R., Young, J.R., 1998. Techniques. In: Bown, P.R. (Ed.), Calcareous Nannofossil Biostratigraphy. Kluwer Academic, London, pp. 16–28.

Brachert, T.C., Agnini, C., Gagnaison, C., Gély, J.P., Henehan, M.J., Westerhold, T., 2023. Astronomical pacing of middle Eocene sea-level fluctuations: Inferences from shallow-water carbonate ramp deposits. Paleoceanogr. Paleoclimatol. 38, e2023PA004633.

Bralower, T.J., 2002. Evidence of surface water oligotrophy during the Paleocene-Eocene thermal maximum: Nannofossil assemblage data from ocean drilling program Site 690, Maud rise, Weddell Sea. Paleoceanography 17 (2), 13-1.

Brandano, M., 2019. The role of oceanographic conditions on Cenozoic carbonate platform drowning: Insights from Alpine and Apennine foreland basins. Terra Nova 31 (2), 102–110. https://doi.org/10.1111/ter.12375.

Brandano, M., Tomassetti, L., 2022. MECO and Alpine orogenesis: Constraints for facies evolution of the Bartonian nummulitic and *Solenomeris* limestone in the Argentina Valley (Ligurian Alps). Sedimentology 69 (1), 24–46. https://doi.org/10.1111/sed.12829.

Briguglio, A., Giraldo-Gómez, V.M., Baucon, A., Benedetti, A., Papazzoni, C.A., Pignatti, J., Wolfgring, E., Piazza, M., 2024. A middle Eocene shallow-water drowning ramp in NW Italy: from shoreface conglomerates to distal marls. Newsl. Stratigr. 5 (1), 37–63. https://doi.org/10.1127/nos/2023/0784.

Capdevila, P., Stott, I., Beger, M., Salguero-Gómez, R., 2020. Towards a comparative framework of demographic resilience. Trends Ecol. Evol. 35 (9), 776–786.

Coccioni, R., Bancalà, G., Catanzariti, R., Fornaciari, E., Frontalini, F., Giusberti, L., Jovane, L., Luciani, V., Savian, J., Sprovieri, M., 2012. An integrated stratigraphic record of the Palaeocene-lower Eocene at Gubbio (Italy), new insights into the early Palaeogene hyperthermals and carbon isotope excursions. Terra Nova 24, 380–386. https://doi.org/10.1111/j.1365-3121.2012.01076.x.

Coletti, G., Mariani, L., Garzanti, E., Consani, S., Bosio, G., Vezzoli, G., Hu, X., Basso, D., 2021. Skeletal assemblages and terrigenous input in the Eocene carbonate systems of the Nummulitic Limestone (NW Europe). Sediment. Geol. 425, 106005. https://doi.org/10.1016/j.sedgeo.2021.106005.

Cooley, S., Schoeman, D., Bopp, L., Boyd, P., Donner, S., Ito, S.I., Kiessling, W., Martinetto, P., Ojea, E., Racault, M.F., Rost, B., Skern-Mauritzen, M., Ghebrehiwet, D.Y., Bell, J.D., Blanchard, J., Cheung, W.W., Bolin, J., Dupont, S., Cisneros-Montemayor, A., Frölicher, T., Dutkiewicz, S., Molinos, J.G., Gaitán-Espitia, J.D., Henson, S., Gurney-Smith, H., Holland, E., Hidalgo, M., Kordas, R., Kopp, R., Le Bris, N., Kwiatkowski, L., Mark, F.C., Mgaya, Y., Lluch-Cota, S.E., Logan, C., Randin, G., Raja, N.B., Moloney, C., Muñoz Sevilla, N.P., Roe, S., Ruiz Diaz, R., Rajkaran, A., Richardson, A., Scales, K., Scobie, M., Salili, D., Sallée, J.B., Yool, A., Torres, O., Simmons, C.T., 2023. Oceans and coastal ecosystems and their services. In: Climate Change 2022: Impacts, Adaptation and Vulnerability. Contribution of Working Group II to the Sixth Assessment Report of the Intergovernmental Panel on climate Change: 379-550. Cambridge University Press. https://doi.org/10.1017/9781009325844.

Coxall, H.K., Wilson, P.A., Pälike, H., Lear, C.H., Backman, J., 2005. Rapid stepwise onset of Antarctic glaciation and deeper calcite compensation in the Pacific Ocean. Nature 433, 53–57. https://doi.org/10.1038/nature03135.

Dallagiovanna, G., Fanucci, F., Pellegrini, L., Seno, S., Bonini, L., Decarlis, A., Maino, M., Morelli, D., Toscani, G., Con Contributi di Breda, A., Vercesi, P.L., Zizioli, D., Cobianchi, M., Mancin, N., Papazzoni, C.A., 2012. Note illustrative della Carta Geologica d'Italia alla scala 1:50000, Foglio 257 e 270 Dolceacqua – Ventimiglia. Regione Liguria e ISPRA, p. 103. https://www.isprambiente.gov.it/Media/carg/note_illustrative/257_270_Dolceacqua_Ventimiglia.pdf.

de Graciansky, P.C., Roberts, D.G., Tricart, P., 2010. The Western Alps, from Rift to Passive Margin to Orogenic Belt: An Integrated Geoscience Overview. In: Developments in Earth Surface Processes 14. Elsevier, Amsterdam, p. 398.

De Rijk, S., Jorissen, F.J., Rohling, E.J., Troelstra, S.R., 2000. Organic flux control on bathymetric zonation of Mediterranean benthic foraminifera. Mar. Micropaleontol. 40 (3), 151–166. https://doi.org/10.1016/S0377-8398(00)00037-2.

Decarlis, A., Maino, M., Dallagiovanna, G., Lualdi, A., Masini, E., Seno, S., Toscani, G., 2014. Salt tectonics in the SW Alps (Italy–France): from rifting to the inversion of the European continental margin in a context of oblique convergence. Tectonophysics 636, 293–314. https://doi.org/10.1016/j.tecto.2014.09.003.

D'Onofrio, R., Luciani, V., 2020. Do different extraction techniques impact planktic foraminiferal assemblages? An early Eocene case study. Mar. Micropaleontol. 101795, 0377–8398. https://doi.org/10.1016/j.marmicro.2019.101795.

D'Onofrio, R., Luciani, V., Fornaciari, E., Giusberti, L., Boscolo Galazzo, F., Dallanave, E., Westerhold, T., Sprovieri, M., Telch, S., 2016. Environmental perturbations at the early Eocene ETM2, H2, and I1 events as inferred by Tethyan calcareous plankton (Terche section, northeastern Italy). Paleoceanography 31 (9), 1225–1247. https://doi.org/10.1002/2016PA002940.

D'Onofrio, R., Zaky, A.S., Frontalini, F., Luciani, V., Catanzariti, R., Francescangeli, F., Jovane, L., 2021. Impact of the Middle Eocene Climatic Optimum (MECO) on foraminiferal and calcareous nannofossil assemblages in the Neo-Tethyan Baskil Section (Eastern Turkey): paleoenvironmental and paleoclimatic reconstructions. Appl. Sci. 11 (23), 11339.

Edgar, K.M., Wilson, P.A., Sexton, P.F., Suganuma, Y., 2007. No extreme bipolar glaciation during the main Eocene calcite compensation shift. Nature 448, 908–911.

Edgar, K.M., Wilson, P.A., Sexton, P.F., Gibbs, S.J., Roberts, A.P., Norris, R.D., 2010. New biostratigraphic, magnetostratigraphic and isotopic insights into the Middle Eocene Climatic Optimum in low latitudes. Palaeogeogr. Palaeoclimatol. Palaeoecol. 297, 670–682. https://doi.org/10.1016/j.palaeo.2010.09.016.

Filippi, G., Barrett, R., Schmidt, D.N., D'Onofrio, R., Westerhold, T., Brombin, V., Luciani, V., 2024. Impacts of the Early Eocene Climatic Optimum (EECO,~ 53-49 Ma) on Planktic Foraminiferal Resilience. Paleoceanogr. Paleoclimatol. 39 (8), e2023PA004820.

Fio, K., Spangenberg, J.E., Vlahović, I., Sremac, J., Velić, I., Mrinjek, E., 2010. Stable isotope and trace element stratigraphy across the Permian-Triassic transition: A redefinition of the boundary in the Velebit Mountain, Croatia. Chem. Geol. 278 (1–2), 38–57.

Fornaciari, E., Giusberti, L., Luciani, V., Tateo, F., Agnini, C., Backman, J., Oddone, M., Rio, D., 2007. An expanded Cretaceous–Tertiary transition in a pelagic setting of the Southern Alps (central–western Tethys). Paleoceanogr. Paleoclimatol. 255, 98–131.

Fornaciari, E., Agnini, C., Catanzariti, R., Rio, D., Bolla, E.M., Valvasoni, E., 2010. Mid latitude calcareous nannofossil biostratigraphy and biochronology across the middle to late Eocene transition. Stratigraphy 7, 229–264.

Gandolfi, A., Giraldo-Gómez, V.M., Luciani, V., Piazza, M., Adatte, T., Arena, L., Brahimsamba, B., Fornaciari, E., Frijia, G., Kocsis, L., Briguglio, A., 2023. The Middle Eocene Climatic Optimum (MECO) impact on the benthic and planktic foraminiferal resilience from a shallow-water sedimentary record. Riv. Ital. Paleontol. Stratigr. 129 (3), 629–651. https://doi.org/10.54103/2039-4942/20154.

Gandolfi, A., Giraldo-Gómez, V.M., Luciani, V., Piazza, M., Brombin, V., Crobu, S., Papazzoni, C.A., Pignatti, J., Briguglio, A., 2024. Unraveling ecological signals related to the MECO onset through planktic and benthic foraminiferal records along a mixed carbonate-siliciclastic shallow-water succession. Mar. Micropaleontol. 190, 102388. https://doi.org/10.1016/j.marmicro.2024.102388.

Giammarino, S., Fanucci, F., Orezzi, S., Rosti, D., Morelli, D., Cobianchi, M., De Stefanis, A., Di Stefano, A., Finocchiaro, F., Fravega, P., Piazza, M., Vannucci, G., 2010. Note Illustrative della Carta Geologica d'Italia alla scala 1:50.000 - Foglio "San Remo" n.258- 271. ISPRA - Regione Liguria. 130 pp. A.T.I. - SystemCart s.r.l. - L.A.C. s.r.l. - S.EL.CA., Firenze.

Gibbs, S., Shackleton, N., Young, J., 2004. Orbitally forced climate signals in mid-Pliocene nannofossil assemblages. Marine Micropaleontol. 51 (1–2), 39–56.

Giorgioni, M., Jovane, L., Rego, E.S., Rodelli, D., Frontalini, F., Coccioni, R., Catanzariti, R., Özcan, E., 2019. Carbon cycle instability and orbital forcing during the Middle Eocene Climatic Optimum. Sci. Rep. 9 (9357), 2019. https://doi.org/10.1038/s41598-019-45763-2.

Giraldo-Gómez, V.M., Beik, I., Podlaha, O.G., Mutterlose, J., 2017. The micropaleontological record of marine early Eocene oil shales from Jordan. Palaeogeogr. Palaeoclimatol. Palaeoecol. 485, 723–739. https://doi.org/10.1016/j.palaeo.2017.07.030.

Giraldo-Gómez, V.M., Mutterlose, J., Podlaha, O.G., Speijer, R.P., Stassen, P., 2018a. Benthic foraminifera and geochemistry across the Paleocene-Eocene thermal Maximum interval in Jordan. J. Foraminifer. Res. 48 (2), 100–120.

Giraldo-Gómez, V.M., Beik, I., Podlaha, O.G., Mutterlose, J., 2018b. A paleoenvironmental analyses of benthic foraminifera from Upper Cretaceous-lower Paleocene oil shales of Jordan. Cretac. Res. 91, 1–13.

Giraldo-Gómez, V.M., Piazza, M., Arena, L., Baucon, A., Gandolfi, A., Papazzoni, C.A., Pignatti, J., Briguglio, A., 2024. A Paleogene mixed carbonate-siliciclastic system in the western Tethys: spectral gamma-ray as a tool for the reconstruction of paleoclimate and transgressive-regressive cycles. Mar. Pet. Geol. 162, 106752. https://doi.org/10.1016/j.marpetgeo.2024.106752.

Hammer, Ø., Harper, D.A.T., Ryan, P.D., 2001. PAST: paleontological statistics software package for education and data analysis. Palaeontol. Electron. 4 (1), 1–9.

Hess, S., Kuhnt, W., 2005. Neogene and Quaternary paleoceanographic changes in the southern South China Sea (Site 1143): the benthic foraminiferal record. Mar. Micropaleontol. 54, 63–87. https://doi.org/10.1016/j.marmicro.2004.09.004.

Hodgson, D., McDonald, J.L., Hosken, D.J., 2015. What do you mean 'resilient'? Trends Ecol. Evol. 30 (9), 503–506.

Holbourn, A., Henderson, A.S., MacLeod, N., MacLeod, N., 2013. Atlas of Benthic Foraminifera, 654. Wiley-Blackwell, London.

Hollis, C.J., Taylor, K.W., Handley, L., Pancost, R.D., Huber, M., Creech, J.B., Hines, B.R., Crouch, E.M., Morgans, H.E.G., Crampton, J.S., Gibbs, S., Pearson, P.N., Zachos, J.C., 2012. Early Paleogene temperature history of the Southwest Pacific Ocean: Reconciling proxies and models. Earth Planet. Sci. Lett. 349, 53–66.

Hönisch, B., Royer, D.L., Breecker, D.O., Polissar, P.J., Bowen, G.J., Henehan, M.J., Cui, Y., Steinthorsdottir, M., McElwain, J.C., Kohn, M.J., Pearson, A., Phelps, S.R., Uno, K.T., Ridgwell, A., Anagnostou, E., Austermann, J., Badger, M.P.S., Barclay, R. S., Bijl, P.K., Chalk, T.B., Scotese, C.R., de la Vega, E., DeConto, R.M., Dyez, K.A., Ferrini, V., Franks, P.J., Giulivi, C.F., Gutjahr, M., Harper, D.T., Haynes, L.L., Huber, M., Snell, K.E., Keisling, B.A., Konrad, W., Lowenstein, T.K., Malinverno, A., Guillermic, M., Mejía, L.M., Milligan, J.N., Morton, J.J., Nordt, L., Whiteford, R., Roth-Nebelsick, A., Rugenstein, J.K.C., Schaller, M.F., Sheldon, N.D., Sosdian, S., Wilkes, E.B., Witkowski, C.R., Zhang, Y.G., Anderson, L., Beerling, D.J., Bolton, C.B., Cerling, T.E., Cotton, J.M., Da, J., Ekart, D.D., Foster, G.L., Greenwood, D.R., Hyland, E.G., Jagniecki, E.A., Jasper, J.P., Kowalczyk, J.B., Kunzmann, L., Kürschner, W.M., Lawrence, C.E., Lear, C.H., Martínez-Botí, M.A., Maxbauer, D.P., Montagna, P., Naafs, B.D.A., Rae, J.W.B., Raitzsch, M., Retallack, G.J., Ring, S.J., Seki, O., Sepúlveda, J., Sinha, A., Tesfamichael, T.F., Tripati, A., van der Burgh, J., Yu, J., Zachos, J.C., Zhang, L., 2023. Toward a Cenozoic history of atmospheric CO_2. Science 382 (6675). https://doi.org/10.1126/science.adi5177.

Huber, M., Caballero, R., 2011. The early Eocene equable climate problem revisited. Clim. Past 7 (2), 603–633.

Inglis, G.N., Farnsworth, A., Lunt, D., Gavin, L., Foster, G.L., Hollis, C.J., Pagani, M., Jardine, P.E., Pearson, P.N., Markwick, P., Galsworthy, A.M.J., Raynham, L., Taylor, K.W.R., Pancost, R.D., 2015. Descent toward the Icehouse: Eocene Sea surface cooling inferred from GDGT distributions. Paleoceanogr. Paleoclimatol. 30 (7), 1000–1020. https://doi.org/10.1002/2014PA002723.

Inglis, G.N., Bragg, F., Burls, N.J., Cramwinckel, M.J., Evans, D., Foster, G.L., Huber, M., Lunt, D.J., Siler, N., Steinig, S., Tierney, J.E., Wilkinson, R., Anagnostou, E., de Boer, A.M., Dunkley Jones, T., Edgar, K.M., Hollis, C.J., Hutchinson, D.K., Pancost, R.D., 2020. Global mean surface temperature and climate sensitivity of the early Eocene Climatic Optimum (EECO), Paleocene-Eocene thermal Maximum (PETM), and latest Paleocene. Clim. Past 16 (5), 1953–1968. https://doi.org/10.5194/cp-16-1953-2020.

Ivany, L.C., Lohmann, K.C., Hasiuk, F., Blake, D.B., Glass, A., Aronson, R.B., Moody, R. M., 2008. Eocene climate record of a high southern latitude continental shelf: Seymour Island,. Antarctica. Geol. Soc. Am. Bull. 120 (5–6), 659–678.

John, E.H., Pearson, P.N., Coxall, H.K., Birch, H., Wade, B.S., Foster, G.L., 2013. Warm ocean processes and carbon cycling in the Eocene. Philosophic. Transact. Royal Soc. A: Mathematic. Physic. Eng. Sci. 371 (2001), 20130099.

John, E.H., Wilson, J.D., Pearson, P.N., Ridgwell, A., 2014. Temperature-dependent remineralization and carbon cycling in the warm Eocene oceans. Palaeogeogr. Palaeoclimatol. Palaeoecol. 413, 158–166.

Jovane, L., Florindo, F., Coccioni, R., Dinarès-Turell, J., Marsili, A., Monechi, S., Roberts, A.P., Sprovieri, M., 2007. The middle Eocene climatic optimum event in the Contessa Highway section, Umbrian Apennines, Italy. Geol. Soc. Am. Bull. 119, 413–427.

Kaiho, K., 1994. Benthic foraminiferal dissolved-oxygen index and dissolved-oxygen levels in the modern ocean. Geology 22 (8), 719–722. https://doi.org/10.1130/0091-7613(1994)022<0719:BFDOIA>2.3.CO;2.

Kawagata, S., Hayward, B.W., Gupta, A.K., 2006. Benthic foraminiferal extinctions linked to late Pliocene-Pleistocene deep-sea circulation changes in the northern Indian Ocean (ODP Sites 722 and 758). Mar. Micropaleontol. 58 (3), 219–242. https://doi.org/10.1016/j.marmicro.2005.11.003.

Kearns, L.E., Bohaty, S.M., Edgar, K.M., Nogué, S., Ezard, T.H.G., 2021. Searching for function: Reconstructing adaptive niche changes using geochemical and morphological data in planktonic foraminiera. Front. Ecol. Evol. 9, 679–722. https://doi.org/10.3389/fevo.2021.679722.

Kleiber, G.W., 1991. Nummuliten der paläogenen Tethys in Axialschnitten. Tübinger Micropaläont. Mitt. 9, 1–262.

Kövecsi, S.A., Less, G., Pleş, G., Bindiu-Haitonic, R., Briguglio, A., Papazzoni, C.A., Silye, L., 2022. Nummulites assemblages, biofabrics and sedimentary structures: The

anatomy and depositional model of an extended Eocene (Bartonian) nummulitic accumulation from the Transylvanian Basin (NW Romania). Palaeogeogr. Palaeoclimatol. Palaeoecol. 586, 110751. https://doi.org/10.1016/j.palaeo.2021.110751.

Lavastre, V., Ader, M., Buschaert, S., Petit, E., Javoy, M., 2011. Water circulation control on carbonate $\delta^{18}O$ records in a low permeability clay formation and surrounding limestones: the Upper Dogger-Oxfordian sequence from the eastern Paris basin, France. Appl. Geochem. 26 (5), 818–827.

Licari, L., 2006. Ecological preferences of benthic foraminifera in the Eastern South Atlantic: distribution patterns, stable carbon isotopic composition, and paleoceanographic implications. Report. Polar Marine Res. 523.

Lirer, F., 2000. A new technique for retrieving calcareous microfossils from lithified lime deposits. Micropaleontology 46, 365–369.

Loeblich, A.R., Tappan, H., 1987. Foraminiferal Genera and their Classification. Van Nostrand Reinhold Company, New York, p. 2045.

Loeblich, A.R., Tappan, H., 1994. Foraminifera of the Sahul Shelf and Timor Sea. Cushman Foundat. Foraminiferal Res. Spec. Pub. 31, 1–661.

Luciani, V., Giusberti, L., 2014. Reassessment of the early–middle Eocene planktic foraminiferal biomagnetochronology: new evidence from the Tethyan Possagno section (NE Italy) and Western North Atlantic Ocean ODP Site 1051. J. Foraminifer. Res. 44, 187–201.

Luciani, V., Giusberti, L., Agnini, C., Backman, J., Fornaciari, E., Rio, D., 2007. The Paleocene-Eocene thermal Maximum as recorded by Tethyan planktonic foraminifera in the Forada section (northern Italy). Mar. Micropaleontol. 64 (3), 189–214. https://doi.org/10.1016/j.marmicro.2007.05.001.

Luciani, V., Giusberti, L., Agnini, C., Fornaciari, E., Rio, D., Spofforth, D.J.A., Pälike, H., 2010. Ecological and evolutionary response of Tethyan planktonic foraminifera to the middle Eocene climatic optimum (MECO) from the Alano section (NE Italy). Palaeogeogr. Palaeoclimatol. Palaeoecol. 292, 82–95. https://doi.org/10.1016/j.palaeo.2010.03.029.

Luciani, V., Dickens, G.R., Backman, J., Fornaciari, E., Giusberti, L., Agnini, C., D'Onofrio, R., 2016. Major perturbations in the global carbon cycle and photosymbiont-bearing planktic foraminifera during the early Eocene. Clim. Past 12, 981–1007. https://doi.org/10.5194/cp-12-981-2016.

Ma, Z., Gray, E., Thomas, E., Murphy, B., Zachos, J., Paytan, A., 2014. Carbon sequestration during the Palaeocene–Eocene Thermal Maximum by an efficient biological pump. Nat. Geosci. 7 (5), 382–388.

Marchegiano, M., John, C.M., 2022. Disentangling the impact of global and regional climate changes during the middle Eocene in the Hampshire Basin: new insights from carbonate clumped isotopes and ostracod assemblages. Paleoceanogr. Paleoclimatol. 37 (2), 1–13.

Marini, M., Patacci, M., Felletti, F., Decarlis, A., McCaffrey, W., 2022. The erosionally confined to emergent transition in a slope- derived blocky mass-transport deposit interacting with a turbidite substrate, Ventimiglia Flysch Formation (Grès d'Annot System, north-West Italy). Sedimentology 69, 1675–1704.

Marshall, J.D., 1992. Climatic and oceanographic isotopic signals from the carbonate rock record and their preservation. Geol. Mag. 129, 143–160. https://doi.org/10.1017/S0016756800008244.

Martín-Martín, M., Guerrera, F., Tosquella, J., Tramontana, M., 2021. Middle Eocene carbonate platforms of the westernmost Tethys. Sediment. Geol. 415, 1–25.

Morelli, D., Locatelli, M., Corradi, N., Cianfarra, P., Crispini, L., Federico, L., Migeon, S., 2022. Morpho-structural setting of the Ligurian Sea: the role of structural heritage and neotectonic inversion. J. Mar. Sci. Eng. 10 (9), 1176, 10.390/jmse10091176.

Murray, J.W., 2006. Ecology and Applications of Benthic Foraminifera. Cambridge Univ. Press, New York.

Pearson, P.N., Shackleton, N.J., Hall, M.A., 1993. Stable isotope paleoecology of middle Eocene planktonic foraminifera and multispecies isotope stratigraphy, DSDP Site 523, South Atlantic. J. Foraminifer. Res. 23, 123–140.

Pearson, P.N., Ditchfield, P.W., Singano, J., Harcourt-Brown, K.G., Nicholas, C.J., Olsson, R.K., Shackleton, N.J., Hall, M.A., 2001. Warm tropical sea surface temperatures in the late Cretaceous and Eocene epochs. Nature 413, 481–488. https://doi.org/10.1038/35097000.

Pearson, P.N., Olsson, R.K., Hemleben, C., Huber, B.T., Berggren, W.A., 2006. Atlas of Eocene Planktonic Foraminifera. In: Cushman Foundation for Foraminiferal Research Special Publication, pp. 41–513.

Pellenard, P., Tramoy, R., Pucéat, E., Huret, E., Martinez, M., Bruneau, L., Thierry, J., 2014. Carbon cycle and seawater palaeotemperature evolution at the Middle-late Jurassic transition, eastern Paris Basin (France). Mar. Pet. Geol. 53, 30–43.

Perch-Nielsen, K., 1985. Cenozoic calcareous nannofossils. In: Bolli, H.M., Saunders, J.B., Perch-Nielsen, K. (Eds.), Plankton Stratigraphy: 427–554. Cambridge University Press, Cambridge.

Peris Cabré, S., Valero, L., Spangenberg, J.E., Vinyoles, A., Verité, J., Adatte, T., Tremblin, M., Watkins, S., Sharma, N., Garcés, M., Puigdefàbregas, C., Castelltort, S., 2023. Fluvio-deltaic record of increased sediment transport during the Middle Eocene Climatic Optimum (MECO), Southern Pyrenees, Spain. Clim. Past 19 (3), 533–554. https://doi.org/10.5194/cp-19-533-2023.

Perotti, E., Bertok, C., d'Atri, A., Martire, L., Piana, F., Catanzariti, R., 2012. A tectonically induced Eocene sedimentary mélange in the West Ligurian Alps, Italy. Tectonophysics 568, 200–214. https://doi.org/10.1016/j.tecto.2011.09.005.

Premoli Silva, I., Jenkins, D.G., 1993. Decision on the Eocene-Oligocene boundary stratotype. Episodes 16 (3), 379–382.

Rathburn, A.E., Willingham, J., Ziebis, W., Burkett, A.M., 2018. A new biological proxy for deep-sea paleo-oxygen: Pores of epifaunal benthic foraminifera. Sci. Rep. 8, 9456.

Raven, J., Caldeira, K., Elderfield, H., Hoegh-Guldberg, O., Liss, P., Riebesell, U., Sheperd, J., Turley, C., Watson, A., 2005. Ocean Acidification Due to Increasing Atmospheric Carbon Dioxide. The Royal Society, London.

Rivero-Cuesta, L., Westerhold, T., Agnini, C., Dallanave, E., Wilkens, R.H., Alegret, L., 2019. Paleoenvironmental changes at ODP Site 702 (South Atlantic): anatomy of the middle Eocene climatic optimum. Paleoceanogr. Paleoclimatol. 34 (12), 2047–2066.

Rögl, F., Spezzaferri, S., 2002. Foraminiferal paleoecology and biostratigraphy of the Mühlbach section (Gaindorf Formation, lower Badenian), Lower Austria. Ann. Naturhist. Mus. Wien 104A, 23–75.

Russo, B., Ferraro, L., Correggia, C., Alberico, I., Foresi, L.M., Vallefuoco, M., Lirer, F., 2022. Deep-water paleoenvironmental changes based on early-middle Miocene benthic foraminifera from Malta Island (Central Mediterranean). Palaeogeogr. Palaeoclimatol. Palaeoecol. 586, 110–722.

Savian, J.F., Jovane, L., Trindade, R.I.F., Frontalini, F., Coccioni, R., Bohaty, S.M., Wilson, P.A., Florindo, F., Roberts, A., 2013. Middle Eocene Climatic Optimum (MECO) in the Monte Cagnero Section, Central Italy. Latinmag Lett. 3 (Special Issue), 1–8.

Schaub, H., 1981. Nummulites et Assilines de la Téthys paléogène. Taxinomie, phylogenèse et biostratigraphie. Mém. Suisses Paléontol. 104-106, 1–236.

Schmiedl, G., Mackensen, A., Müller, P.J., 1997. Recent benthic foraminifera from the eastern South Atlantic Ocean: dependence on food supply and water masses. Mar. Micropaleontol. 32 (3–4), 249–287.

Schmiedl, G., Milker, Y., Mackensen, A., 2023. Climate forcing of regional deep-sea biodiversity documented by benthic foraminifera. Earth-Sci. Rev. 104540.

Sen Gupta, B.K., Machain-Castillo, M.L., 1993. Benthic foraminifera in oxygen-poor habitats. Mar. Micropaleontol. 20, 3–4.

Seno, S., Fanucci, F., Dallagiovanna, G., Maino, M., Pellegrini, L., Vercesi, P.L., Morelli, D., Savini, A., Migeon, S., Cobianchi, M., Mancin, N., Marini, M., Felletti, F., Decarlis, A., Maino, M., Toscani, G., Breda, A., Zizioli, D., 2012. Carta Geologica d'Italia alla scala 1:50000, Foglio 257 Dolceacqua e Foglio 270 Ventimiglia, 32-37. Regione Liguria e ISPRA. https://www.isprambiente.gov.it/Media/carg/257_270_DOLCEACQUA_VENTIMIGLIA/Foglio.html.

Serra-Kiel, J., Hottinger, L., Caus, E., Drobne, K., Ferràndez, C., Jauhri, A.K., Less, G., Pavlovec, R., Pignatti, J., Samsó, J.M., Schaub, H., Sirel, E., Strougo, A., Tambareau, Y., Tosquella, J., Zakrevskaya, E., 1998. Larger foraminiferal biostratigraphy of the Tethyan Paleocene and Eocene. Bull. Soc. géol. France 169, 281–299.

Sexton, P.F., Wilson, P.A., Norris, R.D., 2006. Testing the Cenozoic multisite composite $\delta^{18}O$ and $\delta^{13}C$ curves: New monospecific Eocene records from a single locality, Demerara rise (Ocean Drilling Program Leg 207). Paleoceanogr. Paleoclimatol. 21 (2). https://doi.org/10.1029/2005PA001253.

Sharma, N., Spangenberg, J.E., Adatte, T., Vennemann, T., Kocsis, L., Vérité, J., Castelltort, S., 2024. Middle Eocene Climatic Optimum (MECO) and its imprint in the continental Escanilla Formation, Spain. Clim. Past 20, 935–949. https://doi.org/10.5194/cp-20-935-2024.

Sinclair, H.D., 1997. Tectonostratigraphic model for underfilled peripheral foreland basins: an Alpine perspective. Geol. Soc. Am. Bull. 109, 324–346.

Sluijs, A., Zeebe, R.E., Bijl, P.K., Bohaty, S.M., 2013. A middle Eocene carbon cycle conundrum. Nat. Geosci. 6 (6), 429–434. https://doi.org/10.1038/NGEO1807.

Speijer, R.P., 1994. Extinction and recovery patterns in benthic foraminiferal paleocommunities across the Cretaceous/Paleogene and Paleocene/Eocene boundaries. Geol. Ultraiect. 124, 1–191.

Speijer, R.P., Schmitz, B., 1998. A benthic foraminiferal record of Paleocene Sea level and trophic/redox conditions at Gebel Aweina, Egypt. Palaeogeogr. Palaeoclimatol. Palaeoecol. 137 (1–2), 79–101.

Speijer, R.P., Pälike, H., Hollis, C.J., Hooker, J.J., Ogg, J.G., 2020. The Paleogene period. In: Geological Time Scale 2020. Elsevier, pp. 1087–1140.

Spofforth, D.J.A., Agnini, C., Pälike, H., Rio, D., Fornaciari, E., Giusberti, L., Luciani, V., Lanci, L., Muttoni, G., 2010. Organic carbon burial following the middle Eocene climatic optimum in the central western Tethys. Paleoceanogr. Paleoclimatol. 25 (3), 3210. https://doi.org/10.1029/2009PA001738.

Spötl, C., Vennemann, T.W., 2003. Continuous-flow isotope ratio mass spectrometric analysis of carbonate minerals. Rapid Commun. Mass Spectrom. 17, 1004–1006. https://doi.org/10.1002/rcm.1010.

Thomas, E., Gooday, A.J., 1996. Cenozoic deep-sea benthic foraminifers: tracers for changes in oceanic productivity? Geology 24 (4), 355–358.

van der Boon, A., Kuiper, K.F., van der Ploeg, R., Cramwinckel, M.J., Honarmand, M., Sluijs, A., Krijgsman, W., 2021. Exploring a link between the Middle Eocene Climatic Optimum and Neotethys continental arc flare-up. Clim. Past 17 (1), 229–239.

van der Zwaan, G.J., 1982. Paleoecology of Late Miocene Mediterranean Foraminifera. PhD Thesis,. Utrecht University, Netherlands, p. 199.

van der Zwaan, G.J., Jorissen, F.J., Verhallen, P.J.J.M., Von Daniels, C.H., 1986. Atlantic-European Oligocene to recent *Uvigerina*: taxonomy, paleoecology, and paleobiogeography. Utrecht Micropaleontol. Bull. 35, 7–20.

van der Zwaan, G.J., Duijnstee, A.I., den Dulk, M., Ernst, S.R., Jannink, N.T., Kouwenhoven, T.J., 1999. Benthic foraminifers: proxies or problems? A review of paleoecological concepts. Earth Sci. Rev. 46 (1–4), 213–236.

Varrone, D., 2004. Le prime fasi di evoluzione del bacino di avanfossa alpino: la successione delfinese cretacico-eocenica, Alpi marittime. PhD Thesis (unpublished),. University of Torino.

Veizer, J., Ala, D., Azmy, K., Bruckschen, P., Buhl, D., Bruhn, F., Carden, G.A.F., Diener, A., Ebneth, S., Godderis, Y., Jasper, T., Korte, C., Pawellek, F., Podlaha, O.G., Strauss, H., 1999. $^{87}Sr/^{86}Sr$, $\delta\ ^{13}C$ and $\delta\ ^{18}O$ evolution of Phanerozoic seawater. Chem. Geol. 161 (1), 59–88. https://doi.org/10.1016/S0009-2541(99)00081-9.

Villa, G., Fioroni, C., Pea, L., Bohaty, S., Persico, D., 2008. Middle Eocene–late Oligocene climate variability: calcareous nannofossil response at Kerguelen Plateau, Site 748. Mar. Micropaleontol. 69 (2), 173–192.

Wade, B.S., 2004. Planktonic foraminiferal biostratigraphy and mechanisms in the extinction of *Morozovella* in the late middle Eocene. Mar. Micropaleontol. 51 (1–2), 23–38.

Wade, B.S., Kroon, D., 2002. Middle Eocene regional climate instability: evidence from the western North Atlantic. Geology 30 (11), 1011–1014.

Wade, B., Pearson, P.N., Berggren, W.A., Pälike, H., 2011. Review and revision of Cenozoic tropical planktonic foraminiferal biostratigraphy and calibration to the geomagnetic polarity and astronomical time scale. Earth Sci. Rev. 104, 111–142. https://doi.org/10.1016/j.earscirev.2010.09.003.

Wei, W., Wise Jr., S.W., 1989. Paleogene Calcareous Nannofossil Magnetobiochronology: Results from South Atlantic DSDP Site 516. Mar. Micropaleontol. 14, 119–152. https://doi.org/10.1016/0377-8398(89)90034-0.

Young, J.R., 1998. Neogene nannofossils. Calcareous nannofossil biostratigraphy, 225, 265.

Young, J.R., Bown, P.R., Lees, J.A., 2022. Nannotax3 website. International Nannoplankton Association. Accessed 21 Apr. 2022. URL. www.mikrotax.org/Nannotax3.

Zachos, J.C., Pagani, M., Sloan, L.C., Thomas, E., Billups, K., 2001. Trends, rhythms, and aberrations in global climate 65 Ma to present. Science 292, 686–693.

Zachos, J.C., Dickens, G.R., Zeebe, R.E., 2008. An early Cenozoic perspective on greenhouse warming and carbon-cycle dynamics. Nature 451 (7176), 279–283.